A genetic approach to understanding axonal mitochondrial biology

By

Tzu-Huai Lin

A DISSERTATION

Presented to the Vollum Institute/Neuroscience Graduate Program

and Oregon Health & Science University

School of Medicine

in partial fulfillment of

the requirements for the degree of

Doctor of Philosophy

September 2021

Table of Contents

Acknowledgements

All the work presented in this thesis was performed by myself in Dr. Marc Freeman's laboratory and is the sweet fruit from a close collaboration with Dr. Gaynor A. Smith, a former postdoctoral fellow of the lab and now a principal investigator at Cardiff University, UK. All the Freeman lab members that I have had the privilege to interact with, my dissertation advisory committee, and the OHSU community who have provided reagents, constructive feedback, or both, which I greatly appreciate, have facilitated the completion of this work. I would also like to thank the Looger Lab from the Janelia Research Campus for providing the backbone plasmids for making the ATPsnFR transgenic fly, the Whitworth Lab at the University of Cambridge for the mito-QC transgenic fly, Lukas Neukomm for the MARCM flies, the Baehrecke lab at the University of Massachusetts Medical School for the *atg6* knockout fly, and the Bloomington Drosophila Stock Center, Kyoto Stock Center and Vienna Drosophila Resource Center for the rest of the reagents. Lastly, I would like to express my utmost gratitude to my family for their support in all shapes and forms. I would have not been here in pursuit of my passion if not for them. The thesis you are about to read is modified from the published studies *Smith and Lin et al., Neuron 2019* (doi: 10.1016/j.neuron.2019.04.017) and *Lin et al., PNAS 2021* (doi: 10.1073/pnas.2018770118).

Abstract

Mitochondria are essential organelles for all cell types, especially for neurons, which possess extremely long axons that require the support of mitochondria from cell bodies at great distances. Numerous neurodegenerative diseases are associated with mitochondrial dysfunction, and yet how a neuron maintains a pool of properly sized, functionally sound mitochondria at the correct density throughout large stretches of axons *in vivo* remains enigmatic. Given that many molecules known for mitochondrial regulation were discovered in non-neuronal cells in an *in vitro* setting, whether these molecules can translate into *in vivo* mitochondrial regulation is an open and important question. In this thesis, I utilized the power of *Drosophila melanogaster* and its extensive toolbox developed by the fruit fly community to study how axonal mitochondria are regulated *in vivo*. I performed a high-throughput, unbiased and *in vivo* forward genetic screen to identify new modifiers of axonal mitochondria. After screening >6,000 genomes, four candidates were identified, with one fully characterized and studied, the tumor susceptibility gene 101 (TSG101). I found that neurons in TSG101-mutant flies exhibited elevated mitochondrial numbers and shortened mitochondrial sizes in axons, and the mutant neurons underwent spontaneous degeneration at late stages. TSG101 is best known as a gene in the endosomal pathway, but how it regulates mitochondria was not yet studied.

I dedicate the majority of this thesis to unraveling the mechanism by which TSG101 regulates mitochondria. First, I investigated and found that loss of most other ESCRT components had no effect on mitochondrial morphology, suggesting that TSG101 regulates mitochondrial biology in a non-canonical manner. Next, I tested whether TSG101 modulates mitochondrial turnover such that lack of TSG101 causes blocked mitophagy,

which can be mediated by Parkin/PINK1 or macroautophagy, or both. However, I discovered that blocking Parkin/PINK1-dependent mitophagy and macroautophagy was not to blame for the TSG101 phenotype. I also provided evidence to support the notion that mitophagy and macroautophagy, two major pathways turning over mitochondria in other cells, are dispensable in axons. Interestingly, TSG101 mitochondrial phenotypes were instead caused by activation of PGC-1α/Nrf2-dependent mitochondrial biogenesis, which was mTOR-independent, TFEB-dependent, and required the mitochondrial fission-fusion machinery. Lastly, I attempted to genetically dissect the cause of spontaneous neurodegeneration upon TSG101 ablation. TSG101 has been associated with spongiform neurodegeneration, but the detailed mechanism behind it is unknown. Interestingly, my data suggest that this neurodegeneration occurs through an unknown mechanism independent of mitochondria and of Wallerian and apoptotic signaling pathways. Despite many open questions left to be answered, this work not only provides a glimpse into how neurodegeneration occurs upon the loss of an ESCRT component, but also identifies a new role for TSG101 in inhibiting mitochondrial biogenesis, which is essential for maintenance of mitochondrial numbers and sizes in the axonal compartment.

Chapter 1: Introduction

Introduction 1.1: Mitochondria and neurodegenerative diseases

The mitochondrion is a vital organelle for eukaryotic cells that is thought to originate from alpha-proteobacteria, which were internalized into eukaryotic progenitors via endosymbiosis. Similar to their bacterial ancestor, mitochondria have outer (OMs) and inner membranes (IMs) that separate and form the intermembrane space (the space between the two membranes) and the matrix (the space encapsulated by the inner membrane), in which a small circular mitochondrial genome (mtDNA) is stored. Although the mitochondrion contains its own genome, mtDNA encodes only 13 mitochondrial genes, a tiny fraction of the over 1,500 mitochondrial genes that have been implicated in studies using approaches such as proteomics, genomics, and bioinformatics (Gaston et al., 2009; Mootha et al., 2003; Pagliarini et al., 2008; Sickmann et al., 2003). In other words, mitochondria rely heavily on the nuclear genome of the host cell for support.

The fact that the host cell dedicates such considerable resources to maintain mitochondria underscores the importance to the cell of mitochondrial functions. In the 1930's and 40's, mitochondria were discovered to undergo oxidative phosphorylation (OXPHOS) to efficiently convert products of glycolysis, such as pyruvate and reduced nicotinamide adenine dinucleotide (NADH), to large amounts of the energy molecules adenosine triphosphates (ATP); hence, mitochondria have earned the name "the powerhouse of cells". In addition, more recent research has revealed that mitochondria are also involved in numerous cellular functions besides energy conversion and production, including phospholipid biosynthesis, iron-sulfur cluster biogenesis, β-oxidation of fatty

acids, metabolite exchange/buffering, pyrimidine biosynthesis/storage, production of reactive oxygen species (ROS), and release of apoptotic factors (reviewed in Nunnari and Suomalainen, 2012). Since mitochondria are involved in many biological processes, it is not surprising to find that mitochondrial dysfunction has been associated with an increasingly large number of diseases, including cardiomyopathies, metabolic syndromes, cancer, and, last but not least, neurodegenerative disorders (Hewitt and Whitworth, 2017; Jodeiri Farshbaf and Ghaedi, 2017; Nunnari and Suomalainen, 2012; Park et al., 2018; Salvadores et al., 2017).

Mitochondrial functions are strictly linked to their dynamics. Alteration of mitochondrial dynamics can lead to neurodegenerative disorders. For example, Charcot-Marie-Tooth disease type 2A (CMT2A) and Optic Atrophy 1 are, respectively, caused by loss-of-function mutations of mitofusin 2 (*MFN2*) and optic atrophy gene 1 (*OPA1*), the GTPases that mediate mitochondrial fusion. Alzheimer's Amyloid β (Aβ) oligomerization and mutant huntingtin (*HTT*) accumulation can change mitochondrial fission activity via another GTPase, dynamin-related protein 1 (*DRP1*), leading to the fragmentation of mitochondria that further stymies the mitochondrion's ability to sustain neuronal health and physiology (Cho et al., 2010). Failure in the mitochondrial turnover pathway that involves PTEN-induced kinase 1 (PINK1) and Parkin has been strongly suggested to play a role in Parkinson's Disease (PD), and several mutations in PINK1 and Parkin have been identified to cause familial early-onset PD (Kitada et al., 1998; Valente, 2004). Mutations in optineurin (*OPTN*), a receptor for mitochondrial clearance pathway mitophagy, is linked to glaucoma and amyotrophic lateral sclerosis (ALS) (Wong and Holzbaur, 2015). Lastly, the activities of motor proteins that transport mitochondria back and forth along the axons

can be altered by disease factors such as Aβ, mutant *HTT*, mutant *SOD1* and *TDP43* over-expression (*SOD1* and *TDP43* are associated with ALS) (Magrané et al., 2014). Despite the tight association between mitochondria and neuronal health, how a neuron maintains a pool of functional mitochondria in sufficient density and location throughout large stretches of the axon *in vivo* remains enigmatic. Unravelling the relationship between axons and the mitochondria is of paramount importance to defining the basic cell biological principles of axonal maintenance, and it is likely that such insights will shed light on mechanisms that drive neurodegeneration.

Introduction 1.2: Mitochondrial functions–fission and fusion

Since mitochondria are so intricately linked to many cellular functions, it is important to keep a functional pool of mitochondria according to the needs of the cell. Cells regulate mitochondria through five key processes: fission, fusion, mobility, turnover, and mitochondrial biogenesis. Fission and fusion are the most prominent forces governing mitochondrial dynamics, not only determining the number and size of mitochondria, but also serving as a rheostat for adjustment of mitochondrial function. High fission activity promotes mitochondrial fragmentation, which may lead to high ROS production (Yu et al., 2006), high mitochondrial mobility (Saxton and Hollenbeck, 2012), induction of mitochondrial turnover (Frank et al., 2012), and activation of apoptosis (Youle and Karbowski, 2005). Fusion functions in the opposite way of fission, and that may lead to low mitochondrial mobility (Saxton and Hollenbeck, 2012), maximized activity of ATP synthesis (Mishra et al., 2014), and enhancement of Ca^{2+} buffering (Maltecca et al., 2012).

The fission-fusion equilibrium is achieved through the activity of many GTPases, including Drp1 for fission and mitofusin MFN1/2 (Marf in flies) and OPA1 for fusion.

Fission is a process that requires Drp1 to scissor mitochondria (Fig. 1.1A). Drp1 is a cytosolic protein that belongs to the dynamin family, which possesses membrane-shaping ability. It polymerizes and forms a collar around the tubular mitochondria, and the diameter of this collar is smaller than those of mitochondria. GTP hydrolysis by the GTPase activity of Drp1 further constricts the collar and eventually leads to fission. However, since the poly- Drp1 ring is smaller than the mitochondria, pre-constriction of mitochondria is required. During fission, the endoplasmic reticulum (ER) initiates pre-constriction by extending a tube of ER to physically wrap around the mitochondria. This initiation event provides a site for mitochondrial receptors for Drp1, such as mitochondrial fission factor (Mff) and mitochondrial dynamics proteins (MiDs), to recruit Drp1 to the ER-mitochondrial contact site, further triggering Drp1 assembly and the subsequent execution of membrane scissoring (Elgass et al., 2015; Friedman et al., 2011; Lee and Yoon, 2016).

Mitochondrial fusion, on the other hand, is less well-understood. Fusion of mitochondria is mediated by MFN (either MFN1 or MFN2) on the OMs and OPA1 on the IMs of mitochondria (Koshiba, 2004) (Fig. 1.1B). The full protein structure of MFN is not known, and therefore the detailed molecular mechanism of fusion by MFN is not fully understood, but MFN is thought to tether the OMs of mitochondria at the fusion site and bind to the MFN on the opposing mitochondria. Upon GTP hydrolysis, MFN would undergo conformational change to bring the opposing mitochondrial membranes to proximity, and the GDP release may eventually lead to membrane fusion (Brandt et al., 2016; Lee and Yoon, 2016; Low and Löwe, 2006). Similar to MFN, the detailed protein

structure of OPA1 is also obscure. OPA1 was identified from a human disease, Optic Atrophy 1, and it is a homolog of yeast Mgm1, which localizes on the IMs of mitochondria and mediates mitochondrial fusion. OPA1 has also been shown to regulate the cristae structure of mitochondria. OPA1 can be cleaved by the metalloproteases OMA1 and Yme1L. As a consequence, cells contain both the long form (L-OPA1) and the short, cleaved form of OPA1 (S-OPA1). The predicted structure of S-OPA1 is similar to that of Drp1. The general consensus now is that L-OPA1 mediates fusion and S-OPA1 fission, although this is still debatable due to conflicting experiments in the field (reviewed in Lee and Yoon, 2016). Overall, more detailed structural information of Mfn and OPA1 is required for a full picture of how mitochondrial fusion works, and additional factors for both fission and fusion are waiting to be explored.

Introduction 1.3: Mitochondrial functions–mobility

In addition to fission and fusion, mitochondrial mobility is another way to regulate mitochondria. In both *in vitro* and *in vivo* settings, two distinct populations of mitochondria have been observed: motile and stationary. The motile mitochondria that move along on microtubules may pause temporarily but tend to keep moving and rarely change their overall direction. Anterograde movement is mediated by the kinesin motors, and dynein/dynactin drives retrograde mobility. Besides kinesin and dynein, a motor adapter complex that constitutes membrane-anchored Miro and motor-binding Milton is also required (Plucińska and Misgeld, 2016; Saxton and Hollenbeck, 2012; Schwarz, 2013) (Fig. 1.1C). This adapter complex is present on both the motile and stationary mitochondria and is susceptible to high Ca^{2+} levels. Mitochondria can be stopped by high levels of local Ca^{2+},

by post-translational modification of microtubules that mitochondria travel on, or by the presence of anchoring proteins such as Syntaphilin (SNPH) (Sheng, 2014). Mobilization of mitochondria by knocking out SNPH elevates ATP levels and, in neuronal contexts, increases presynaptic variability, revealing an intriguing relationship between mitochondrial movement and synaptic plasticity (Sun et al., 2013).

The connection between mitochondrial mobility and mitochondrial fission and fusion is an interesting one. One can envision that the larger the size of the mitochondria, the harder it is for them to move. Indeed, manipulations that result in unusually large mitochondria hinder mitochondrial trafficking (Chang and Reynolds, 2006; Fukumitsu et al., 2016). Moving mitochondria are also found more likely to fuse (Liu et al., 2009; Twig et al., 2010). Even more intriguingly, Drp1 can facilitate bidirectional mitochondrial transport via interacting with either kinesin-1 (Giovarelli et al., 2020) or the dynein-dynactin complex (Drerup et al., 2017). MFN2, a CMT2A-associated protein well-known for mitochondrial fusion, can form a complex with Miro and facilitate mitochondrial transport (Baloh et al., 2007; Misko et al., 2010). The evidence for the functional connection between mitochondrial mobility and fission-fusion is still growing. We shall undoubtedly see more evidence that provides new perspectives in the future.

Introduction 1.4: Mitochondrial functions–mitochondrial turnover

Cells maintain a constant level of functional mitochondrial proteins by reaching a balance between mitochondrial turnover and mitochondrial biogenesis. Four pathways have been identified to turn over mitochondria or the proteins therein (Fig. 1.2). The first pathway uses AAA+ proteases that reside within the mitochondrial matrix and IMs (facing

both the matrix and the intermembrane space) to degrade individual proteins (Glynn, 2017) (Fig 1.2A). This pathway is presumed to exist in all mitochondria regardless of where the mitochondria reside, and thus is considered the first-line defense of mitochondrial protein quality control.

The second pathway removes small portions of mitochondria via mitochondria-derived vesicles (MDV), which is mostly studied in non-neuronal settings (Roberts et al., 2016; Shlevkov and Schwarz, 2014) (Fig. 1.2B). MDVs are single- or double-membraned vesicles that bud off from mitochondria and that can be targeted to lysosomes, peroxisomes, or exosomes (Matheoud et al., 2016; Neuspiel et al., 2008; Soubannier et al., 2012). How MDVs form and what triggers the formation is largely unknown, but some types of MDVs are found to depend on mitophagy proteins Parkin and PINK1 (more about Parkin and PINK in the next paragraph) and the fission protein Drp1; some Drp1-independent MDVs rely on Rab9 and sorting nexin SNX-9 instead (Matheoud et al., 2016; McLelland et al., 2014; Misgeld and Schwarz, 2017; Soubannier et al., 2012).

Both the third and fourth pathways require autophagy machinery, but the detailed mechanisms are different. The third pathway is mitophagy, a mitochondria-targeted autophagy that requires receptors such as Parkin, PINK1 and OPTN for autophagosomes to recognize and wrap individual mitochondria (Fig. 1.2C). Mitophagy was first identified in non-neuronal cells; although Parkin/PINK1-mediated mitophagy does occur in axons of cultured neurons (Ashrafi et al., 2014), whether it also mediates axonal mitochondrial turnover in physiological conditions *in vivo* is not clear. When mitochondria become dysfunctional, either by losing membrane potential or by the presence of misfolded or unfolded proteins, PINK1 accumulates on the mitochondrial membrane and recruits Parkin

to initiate mitophagy, wherein Parkin ubiquitylates proteins on the mitochondrial surface in order for OPTN to recognize the doomed mitochondria and further recruit the autophagy machinery for lysosome-dependent degradation (Chen and Dorn, 2013; Evans and Holzbaur, 2020; Narendra et al., 2008, 2010; Stavoe and Holzbaur, 2019; Sung et al., 2016). This Parkin/PINK1/OPTN-mediated mitophagy demands high levels of ATP; low ATP levels halts the mitophagic process (Cai et al., 2012; Van Laar et al., 2011). There are also alternative mitophagy pathways that are either Parkin-, PINK1-, or even autophagy-independent (Roberts et al., 2016). The relationships among all these alternatives remain elusive.

Lastly, the fourth pathway utilizes macroautophagy that engulfs a portion of the cytoplasm that contains mitochondria (Fig. 1.2D). This pathway requires no special receptors such as Parkin or PINK1, and it arises predominantly from distal axonal regions, including growth cones and synaptic terminals (Maday and Holzbaur, 2014; Misgeld and Schwarz, 2017; Stavoe and Holzbaur, 2019). All four pathways regulate the quality control of mitochondria, but which one contributes the most to maintain a functional pool of mitochondria in different compartments of the neuron remains to be studied.

Introduction 1.5: Mitochondrial functions–mitochondrial biogenesis

As mentioned, mitochondria rely on the nuclear genome to provide 99% of the proteins, and therefore nucleus-based gene expression by transcriptional co-activators and transcription factors is required. To grow and sustain a proper number of functional mitochondria, mitochondria undergo fission, which produces new mitochondria from existing ones. In addition, the master transcriptional co-activator PGC-1α/β and its binding

partner transcription factors, such as NRF1/2 (nuclear respiratory factors), ERRs (estrogen-related receptors), and YY1, are also required to express mitochondrial genes to keep newly generated mitochondria refreshed with functional proteins. By facilitating the activities of the transcription factors, the PGC-1 family is sufficient to increase mitochondrial mass as well as increase the production of ROS-scavenging enzymes, components in OXPHOS chain, and proteins involved in fission-fusion and mitochondrial protein import. Many signaling molecules or pathways can potentiate PGC-1α, in turn activating mitochondrial biogenesis, including AMP activating protein kinase (AMPK), cAMP pathway, and the mTOR pathway (reviewed in Dominy and Puigserver, 2013). Despite the knowledge of the molecules and pathways involved, the full picture of how mitochondria are rejuvenated in different compartments of the neuron is unclear, and how mitochondrial biogenesis coordinates with other regulatory processes such as fission-fusion and mitophagy in the context of a neuron is still a mystery.

Introduction 1.6: Mitochondrial maintenance in axons

All the aforementioned key processes closely crosstalk to achieve sound mitochondrial regulation. Defects in any of the processes can lead to neurological disorders (as mentioned in Introduction 1.1). While many molecules have been found to be involved in regulating individual mitochondria, the detailed mechanisms for maintaining a functional pool of mitochondria at the scale of a neuron *in vivo* are not known. Many of these molecules were discovered in non-neuronal cells in an *in vitro* setting, but the highly polarized architecture of *in vivo* neurons presents a unique challenge in distributing these organelles to support cellular physiology. For instance, the axons of the glutamatergic

sensory neurons in the *Drosophila* L1 wing can reach up to 100 times the length of the soma, whereas in sciatic nerve motor neurons the ratio is 20,000:1 and other animals such as whales have even higher soma-to-axon length ratios (Smith, 2009). These neurons, like all cells, are constrained by molecular and cellular limitations. Most proteins have turnover rates of days to weeks, but the lifespans of neurons in living organisms can be months to decades. No matter how far from the nucleus, the axonal mitochondria still rely on the cell body to supply 99% of the mitochondrial proteins. Moreover, 60-90% of the mitochondria in axons are stationary, and the ones that move have a measured speed so slow that the time it requires for a mitochondrion to travel from a cell body to a synaptic terminal can be longer than the estimated lifespans of mitochondrial proteins in species with large neurons (Misgeld and Schwarz, 2017). These observations raise several questions regarding cellular logistics. Does a soma of <100μm in size have the protein synthesis capacity to support all the mitochondria in the axons that can be meters long? If not, what are the other sources of protein supply? How are mitochondrial proteins turned over in axons? How are axonal mitochondrial number and size regulated? What determines mitochondrial localities in axonal arbors? How many mitochondria should be generated according to either the geometry of the neuron or the peripheral local demands such as synaptic plasticity? In short, all neurons in different shapes and sizes need functional mitochondria in order to support axonal physiology, and yet how the large pool of axonal mitochondria is maintained still largely evades our comprehension. To address these questions, we designed a forward genetic screen utilizing the power of *Drosophila* genetics, aiming at unravelling novel molecules or mechanisms for mitochondrial modulation in axons *in vivo*.

Introduction 1.7: Thesis overview

This thesis describes the forward genetic screen of >6,000 genomes, utilizing glutamatergic sensory neurons in the *Drosophila* wing to search for modulators of axonal mitochondrial dynamics. Chapter 2 presents the details of the screen, in which I randomly mutagenized nuclear genes in flies and screened for candidates that exhibited changes in axonal mitochondrial dynamics and/or morphology. Descriptions of the four mutation lines that have been isolated from the screen are presented in Chapter 2 as well. Tumor susceptibility gene 101 (TSG101) is revealed as a new mitochondrial regulator, and is the most investigated in this thesis; axons that are mutant for TSG101 exhibit the phenotype of elevated mitochondrial number, reduced mitochondrial length, and spontaneous neurodegeneration in the late stage of adulthood. Chapter 3-5 are dedicated to identifying the mechanisms by which TSG101 regulates axonal mitochondria, and Chapter 6 attempts the elucidation of the basis of the neurodegeneration induced by loss of TSG101.

As TSG101 is best known as a component of the endosomal sorting complexes required for transport (ESCRT) machinery in the endosomal pathway, I investigate in Chapter 3 the role of other ESCRT genes in regulating mitochondria. Chapter 4 further investigates whether the observed mitochondrial phenotype is the outcome of blocked mitophagy or mitochondrial clearance. Chapter 4 also reveals, however, that blocking either PINK1/Parkin-mediated mitophagy or macroautophagy exerts no significant detrimental effect on mitochondrial numbers and axonal health, suggesting mitophagy and autophagy are dispensable in the axons. After careful examination of this process in Chapter 5, the results instead suggest that the mutant mitochondrial phenotype is caused by activated mitochondrial biogenesis, indicating a constant suppression of mitochondrial

biogenesis by TSG101 in normal physiological conditions. Lastly, Chapter 6 presents evidence to support the notion that the neurodegeneration caused by TSG101 ablation is independent of mitochondria and other known neuronal death signaling pathways, and therefore the mechanism of this TSG101-dependent degeneration is still unresolved. Overall, I argue that TSG101 is a critical and novel regulator of axonal mitochondrial populations, and that canonical PINK1/Parkin and autophagy-dependent mechanisms for mitochondrial turnover do not predominate in the axonal compartment *in vivo*.

Figures

Fig. 1.1: Mechanisms that regulate mitochondrial dynamics.

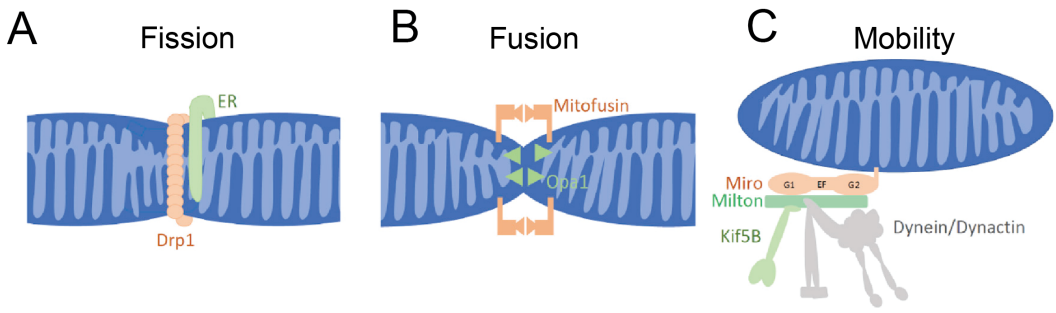

Fig 1.1:

This figure is adapted from the review (Misgeld and Schwarz, 2017). **(A)** Fission of both inner and outer mitochondrial membrane requires initial wrapping of the endoplasmic reticulum (ER) and the subsequent polymerization of Drp1 around the mitochondria. **(B)** Full fusion of mitochondrial outer and inner membrane requires mitofusin and OPA1, respectively. Fusion is initiated by the interaction of mitofusins on opposing mitochondria, leading to outer membrane fusion. The inner membrane undergoes fusion that is mediated by OPA1. **(C)** Mitochondria acquire their mobility by attaching to the motors (kinesin (Kif5B) for the anterograde direction and dynein/dynactin for the retrograde) via the adaptor complex (Miro + Milton).

Fig. 1.2: Mechanisms of mitochondrial turnover.

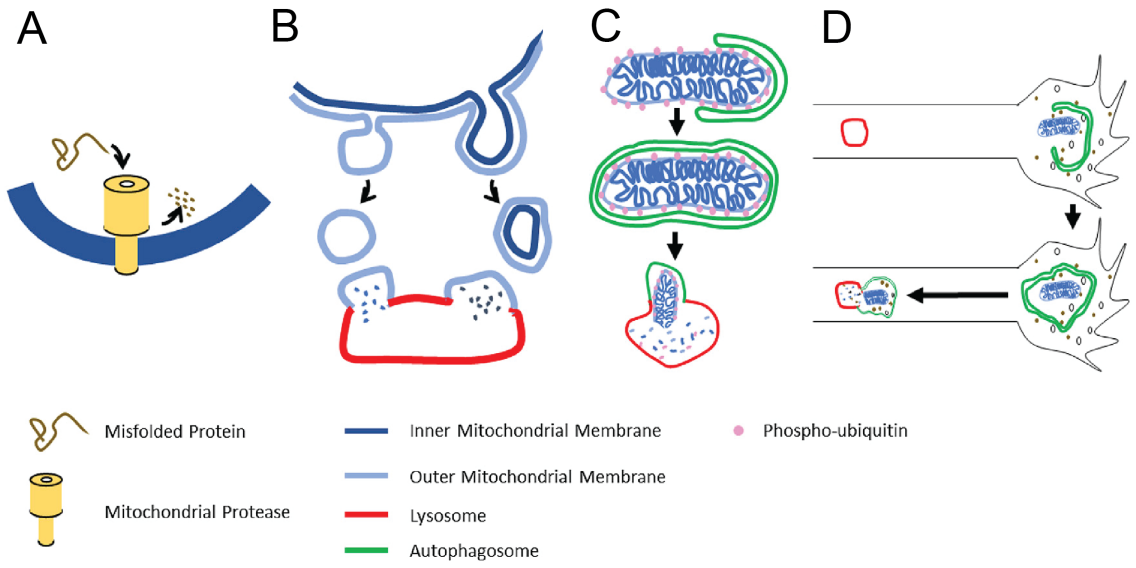

Fig. 1.2:

This figure is adapted from the review (Misgeld and Schwarz, 2017). Mitochondrial quality control comprises four mechanisms **(A)** Individual misfolded or damaged proteins can be degraded by the AAA+ protease residing on the mitochondrial inner membrane. **(B)** Small portions of mitochondria can be shed off via MDVs that either contains only the outer membrane or also the inner membrane and the matrix. **(C)** Mitophagy is initiated by Parkin and PINK1 adding phospho-ubiquitin to the surface of mitochondria. The ubiquitylated mitochondria will be recognized by the autophagy machinery and induce autophagosomal membrane formation. **(D)** Marcoautophagy in growth cones engulfs mitochondria along with other cytoplasmic components. The formed autophagosome travels retrogradely to fuse with lysosomes in axons for degradation.

Chapter 2: Mutagenesis screen for changes in mitochondrial morphology and identification of TSG101 as a new mitochondrial regulator

Results

I set out to look for novel genes or mechanisms in axonal mitochondrial regulation by performing an *in vivo* forward genetic screen. Together with a former post-doctoral fellow, Gaynor A. Smith, we designed and performed the following screen that utilized the genetic toolbox of the clonal system, or mosaic analysis with a repressible cell marker (MARCM) system (Fig. 2.1A-C) (Lee and Luo, 1999; Smith and Lin et al., 2019). In the MARCM-based approach, P0 male flies are mutagenized with ethyl methanesulfonate (EMS), and homozygous mutant glutamatergic neurons in the L1 wing vein of *Drosophila melanogaster* are sparsely generated and labeled (with myr::td-Tomato labeling the neuronal membrane and mito::EGFP labeling the mitochondria) in the heterozygous background of the F1 generation (Fig. 2.1A-C). This approach not only allows for single axon resolution using fluorescent microscopy, but also allows us to discover genes that would otherwise be homozygous lethal, by looking only at homozygous mutations in a subset of neurons. Potential new mitochondrial-regulating molecules were identified based on changes in mitochondrial morphology, number or distribution in either the axon or the cell body, or both.

After screening ~8,000 mutants, Gaynor identified Gfzf as a glutathione transferase (GST) that negatively regulates mitochondrial fusion. Axons that are Gfzf mutant

contained unusually long mitochondria. *gfzf* is a *Drosophila* gene that possesses a zinc-finger domain in addition to the GST one, but it is the GST activity that regulates axonal mitochondrial homeostasis. Gfzf is functionally as conserved and important as other GSTs, including dGSTO1 in *Drosophila* and hGSTT1 in humans; in fact, homozygous mutation of *gfzf* led to lethality of the animal. By utilizing both *Drosophila* and mouse cortical neuronal culture, we found that loss of GSTs in the glutathione pathway led to high levels of oxidized glutathione, or glutathione disulfate GSSG, that in turn activated mitofusin and hence mitochondrial fusion; however, genetic manipulations that reduced GSSG levels rescued this phenotype. Therefore, we discovered the role of Gfzf in maintaining the balance between glutathione and oxidized glutathione (GSH:GSSG) in order to suppress excessive mitochondrial fusion that is redox-mediated and mitofusin-dependent in axons (see Appendix). This work revealed a new role of GSTs in the regulation of mitochondrial morphology, providing a molecular insight into how redox state can change fission-fusion equilibrium. I worked intensively on this project with Gaynor, and was a co-first author on this study when we published it (Smith and Lin et al., 2019).

I contributed to the screen by screening 2,432 mutants on the second chromosome (1,039 on 2L and 1,393 on 2R) and 3,848 on the third (1,712 on 3L and 2,136 on 3R) (see genotypes and cross schemes for each chromosome in Fig 2.1B, C), and identified four mutant lines—*2L.409*, *2L.306*, *3R.1054* and *3L.387* (Fig. 2.1D). *2L.409* was the least characterized due to its phenotype. It was homozygous lethal and the lethality co-segregated genetically with the mutant phenotype. It exhibited a mild mitochondrial phenotype and a pronounced neuronal one. The mutant cell bodies were ballooned and filled with a great number of vesicular structures that were myr::td-Tomato positive (Fig.

2.1Dii); moreover, a small portion of the mutant neurons started degenerating at 7 days post eclosion (7 dpe) (data not shown). As the neuronal phenotype was stronger than the mitochondrial one before neuronal health deteriorated, I suspected mitochondrial defects were secondary to neuronal dysfunction, and so turned my attention to the other mutants.

2L.316 mutants contained exceedingly long mitochondria in both the axons and the cell body (Fig. 2.1Diii). My 1st-round outcrossing result suggested that *2L.316*'s homozygous lethality was associated with the mutant phenotype. Both deficiency mapping and next-generation whole genome sequencing revealed many candidate genes, but Drp1, well-known for its role in mitochondrial fission, was the only one that both techniques found. *2L.316* contains a Proline-to-Leucine amino acid change (P498L), a mutation in a very conserved dynamin stalk domain of Drp1. However, although both of the alleles that are publicly available ($Drp1^{1}$ and $Drp1^{2}$) caused increased mitochondrial length (Smith et al., 2019), their causal lesions are unknown; moreover, both $Drp1^{1}$ and $Drp1^{2}$ are homozygous viable, possibly due to their weak allelic nature compared to *2L.316*; therefore, complementation testing was not feasible. The best way for further characterization of *2L.316* was to generate a transgenic fly that contains the P498L mutation in the dynamin stalk domain of Drp1 by using the CRISPR-Cas9 genome-editing technique. However, due to the extensive existing knowledge of Drp1 function, I decided to turn my attention to *3L.387* below, that affected a novel mitochondrial regulator that will be described in length.

3R.1054 exhibited a phenotype of elevated mitochondrial number and massive cell body size (Fig. 2.1Div). After outcrossing, *3R.1054* was homozygous lethal, and the lethality was always associated with the mutant phenotype. Deficiency mapping revealed many candidate genes, but only the null allele of Tsc1, $Tsc1^{1149}$, failed to complement with

3R.1054. Both knockout of Tsc1 using $Tsc1^{1149}$ and knockdown of Tsc1 via RNAi in later experiments (Fig. 5.3D-F) showed a similar phenotype, further indicating that the causal mutation is in Tsc1. Tsc1 is a well-known inhibitor of the mTOR pathway, which has been confirmed in studies to activate mitochondrial biogenesis and cell growth (Cunningham et al., 2007; Dominy and Puigserver, 2013). In addition, loss of Tsc1 is sufficient to activate mitochondrial biogenesis (Chen et al., 2008). As with Drp1, there is an extensive body of knowledge on the role of Tsc1 in regulating mitochondrial biogenesis. I therefore stopped characterizing *3R.1054*; however, my identification of both Drp1 and Tsc1 in my screen validates the efficiency of my screening approach in identifying important *in vivo* regulators of mitochondrial biology.

For the remainder of my thesis, I will focus on *3L.387*. *3L.387* was homozygous lethal, and the lethality also always genetically co-segregated with the mutant phenotype. Axons in *3L.387* showed elevated mitochondrial number and shortened mitochondrial length (Fig. 2.1Dv). Whole genome sequencing revealed a C-to-T substitution that generated a Q269term mutation in the region encoding the coiled-coil domain of TSG101 (Fig. 2.2B). *3L.387* failed to complement not only with $tsg101^{942}$, a known loss-of-function allele of TSG101, but also with all the available deficiencies that uncover TSG101 in the complementation tests (Fig. 2.2A). Neurons that were $tsg101^{942}$ mutant or knocked down for TSG101 with RNAi in the later experiment (Fig. 5.5A-C) exhibited similar phenotype as in *3L.387*; in addition, re-expression of TSG101 via genomic bacterial artificial chromosome duplication construct (gDNA BAC) suppressed the mutant phenotype (Fig. 2.2), supporting the notion that *3L.387* is a loss-of-function allele of TSG101. Therefore, I later named it $tsg101^{387}$. As mutations in TSG101 caused early larval lethality, all mutant

phenotypes were studied in neuronal clones. At 14 dpe, while controls averaged 9.4 mitochondria per 90 μm of an axon, *tsg101*^{387} mutant neurons contained 21.8 mitochondria (Fig. 2.2C). Although the mitochondrial size was reduced by over 30% in *tsg101*^{387} mutants (Fig. 2.2D), the overall axonal occupation by mitochondria increased by almost 40% (Fig. 2.2E). This change in mitochondrial morphology manifested as early as 1 dpe, and phenotypic differences widened as time elapsed (Fig. 2.3A-C). In addition to the mitochondrial phenotype, I also observed a neuronal one, in which the cell bodies of the mutant neurons were consistently larger than controls (Fig. 2.3D), and neurons underwent spontaneous neurodegeneration at 30 dpe (Fig. 2.3A). Lastly, I found a dramatic increase in endolysosomes (labeled with Lamp1::GFP) in both the axons and the cell bodies of the mutant neurons, and the mutant axons exhibited more stationary endolysosomes in proximity to the mitochondria than the controls did (Fig. 2.4), indicating the importance of TSG101 for maintaining mitochondrial morphology, neuronal integrity, and endolysosomal homeostasis.

Among all the phenotypes caused by TSG101 loss, the change in mitochondrial number and size is the most intriguing. TSG101 has been implicated in neurodegeneration (Jiao et al., 2009) and endolysosomal trafficking (Babst et al., 2000; Kim et al., 2007), but it has not been linked to mitochondrial regulation whatsoever. The following chapters are therefore dedicated to unravelling the mechanisms by which TSG101 alters mitochondrial numbers and sizes, and whether the alteration in mitochondrial morphology is the culprit behind TSG101-dependent neurodegeneration.

Materials & Methods

Mutagenesis screen

Induction of MARCM clones in *Drosophila* wings was described in our previous work (Smith et al., 2019), which is adapted from an axon destruction screen (Neukomm et al., 2014). The screen started off by starving the P0 males (Fig. 2.1) for 8 hours followed by feeding with 25 mM ethyl methanesulfonate (Sigma-Aldrich, Cat#M0880) in 1% sucrose for 12 hours. The mutagenized males were transferred to fresh vials for 12 hours before mating with the P0 virgin females (Fig. 2.1). The F1 progeny, grown in 25℃, were checked at 7 days post eclosion (7 dpe) by clipping off the wings and mounting them in Halocarbon Oil 27 (Sigma-Aldrich, Cat#H8773) on a microscopy slide with a coverslip on top, and immediately examining them under a microscope. Flies with alterations in mitochondrial morphology or dynamics in the axons of the L1 vein were saved, bred, outcrossed, and made into stocks for further characterization, including deficiency mapping and whole-genome sequencing.

Whole-genome sequencing

The nature of gene mutations responsible for mitochondrial phenotypes were identified by next-gen whole-genome sequencing. Genomic DNA was extracted from more than 200 heterozygous adult flies, then sequenced via a HiSeq2000 sequencing system (Illumina). Further analysis to identify mutations and variants was carried out at the Center for Genome Technology, University of Miami.

Microscopy and data analysis

Images were acquired from a Zeiss spinning disc confocal microscope with its proprietary Zen Blue software. Image processing was done with Zen Blue and Fiji (version 2.1.0) (Schindelin et al., 2012). Fiji was used to quantify mitochondrial number and length. All statistical analyses were conducted by using Graph Pad Prism 8. Data in Fig 2.2 were analyzed via one-way ANOVA, with at least 20 wings (one wing/animal) examined for each genotype (N≥20). Data withing the same time point in Fig 2.3 were analyzed via unpaired student t-test, with st least 15 wings (one wing/animal) examined for each genotype (N≥15). Around 10 wings (one wing/animal) were examined in each genotype in Fig 2.4 (N≅10), and were analyzed via unpaired student t-test.

Drosophila *strains*

Detailed genotypes and the cross scheme for the forward genetic screen is described in Fig. 2.1. *Drosophila* strains for Chromosome III mutagenesis and MARCM clone generation were: *OK371-Gal4* (BDSC:26160), *10xUAS-IVS-myr::td-Tomato* (BDSC:32222), *5xUAS-mito::EGFP* (BDSC:8442), *asense-FLP2e* (lab stock), *tub-Gal80* (BDSC:5190, BDSC:5135), *FRT2A* (left arm, BDSC:1997), and *FRT82B* (right arm, BDSC:2035). Fly lines used for Chromosome II mutagenesis and MARCM clone generation were: *nSyb-Gal4* (BDSC:51635), *FRT40A* (left arm, BDSC:1646), *FRTG13* (right arm, BDSC:1956), *asense-FLP3b* (lab stock), *tub-Gal80* (BDSC:5192, BDSC:5140), *10xUAS-IVS-myr::td-Tomato* (BDSC:32221), and *5xUAS-mito::GFP* (BDSC:8443). Fly strains for live-imaging of endolysosomes were: *OK371-Gal4*, *5xUAS-Lamp1::EGFP* (BDSC:42714), *5xUAS-mito::td-Tomato* (lab stock, Smith et al., 2019)*, asense-FLP2e; tub-Gal80*, *FRT2A*, and *FRT82B*. All the autosome deficiencies for deficiency mapping

were from the Bloomington *Drosophila* Stock Center (BDSC). Other flies used for TSG101 characterization are: $tsg101^{942}$ (BDSC:63105) and $BAC_{CH322\text{-}97B15}$ (covering *tsg101*, GenetiVision; Stock ID:P9-D10).

Figures

Fig. 2.1: The MARCM-based mutagenesis screen and candidates of mitochondrial modulators.

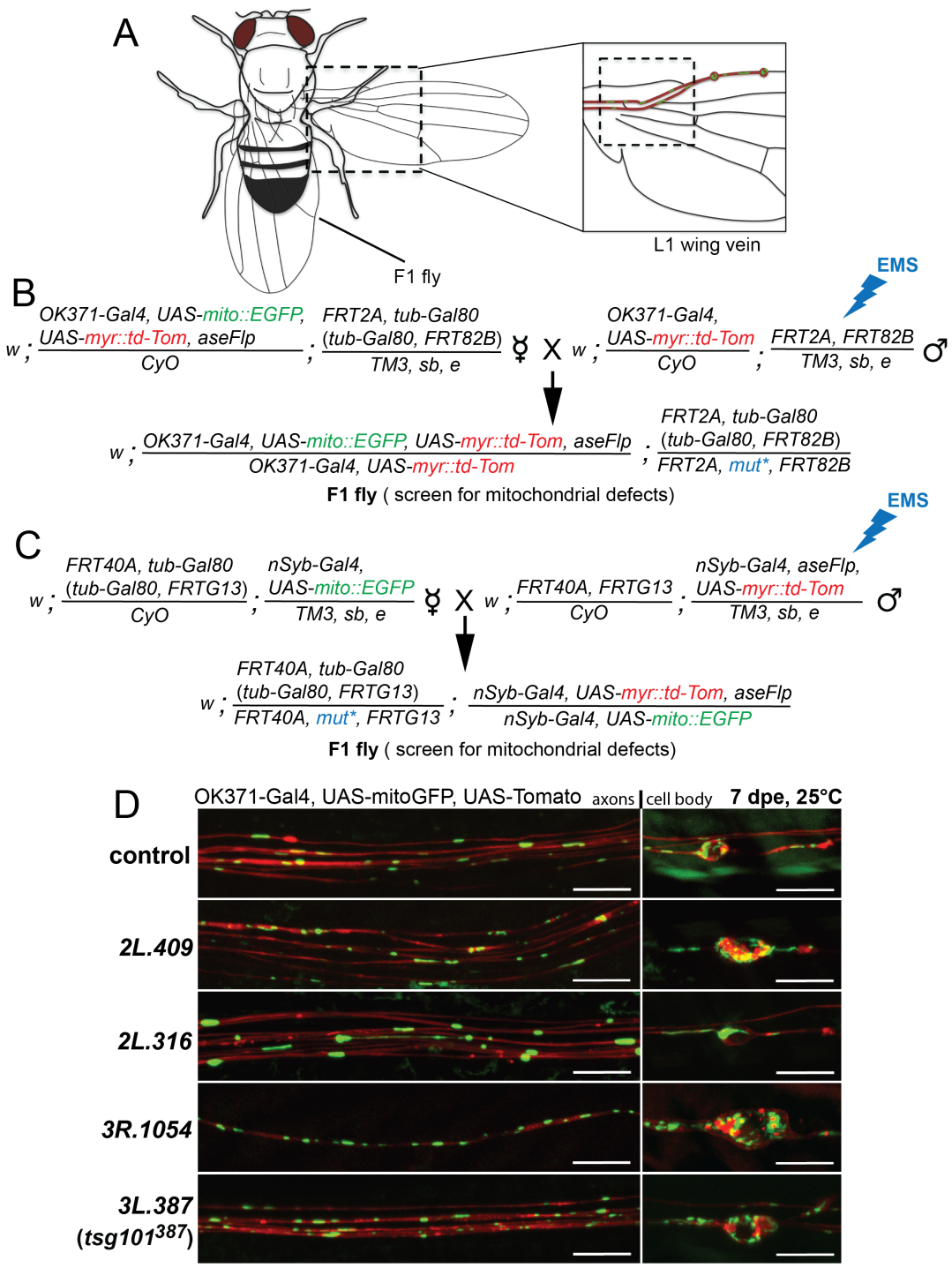

Fig. 2.1:

(A) A diagram of *Drosophila melanogaster* and the neurons used for the mutagenesis forward genetic screen, in which homozygous mutant neurons are generated with the MARCM technique and labeled with myr::td-Tomato (red) and mitochondria mito::EGFP (green). **(B, C)** Cross schemes of the MARCM-based screen for the third-chromosome (B) and the second-chromosome (C). In both setups, P0 males were fed with the mutagen ethyl methanesulfonate (EMS) and crossed to P0 virgin females that contained the genetic elements for the MARCM clone induction. FRT2A was used for the left arm of the third chromosome (3L), FRT82B the right arm of the third (3R), FRT40A 2L, and FRTG13 2R. The F1 progenies with all the required genetic elements and possible mutation (mut*) were checked under the fluorescence microscope at 7 dpe. **(D)** Mutation lines isolated from the screen. *2L.409* and *2L.306* were identified from the 2L screen, *3R.1054* from the 3R, and *3L.387* from the 3L, with no candidate identified in 2R. Scale bar: 10 μm.

Fig. 2.2: Characterization of *3L.387/tsg101*^{387}.

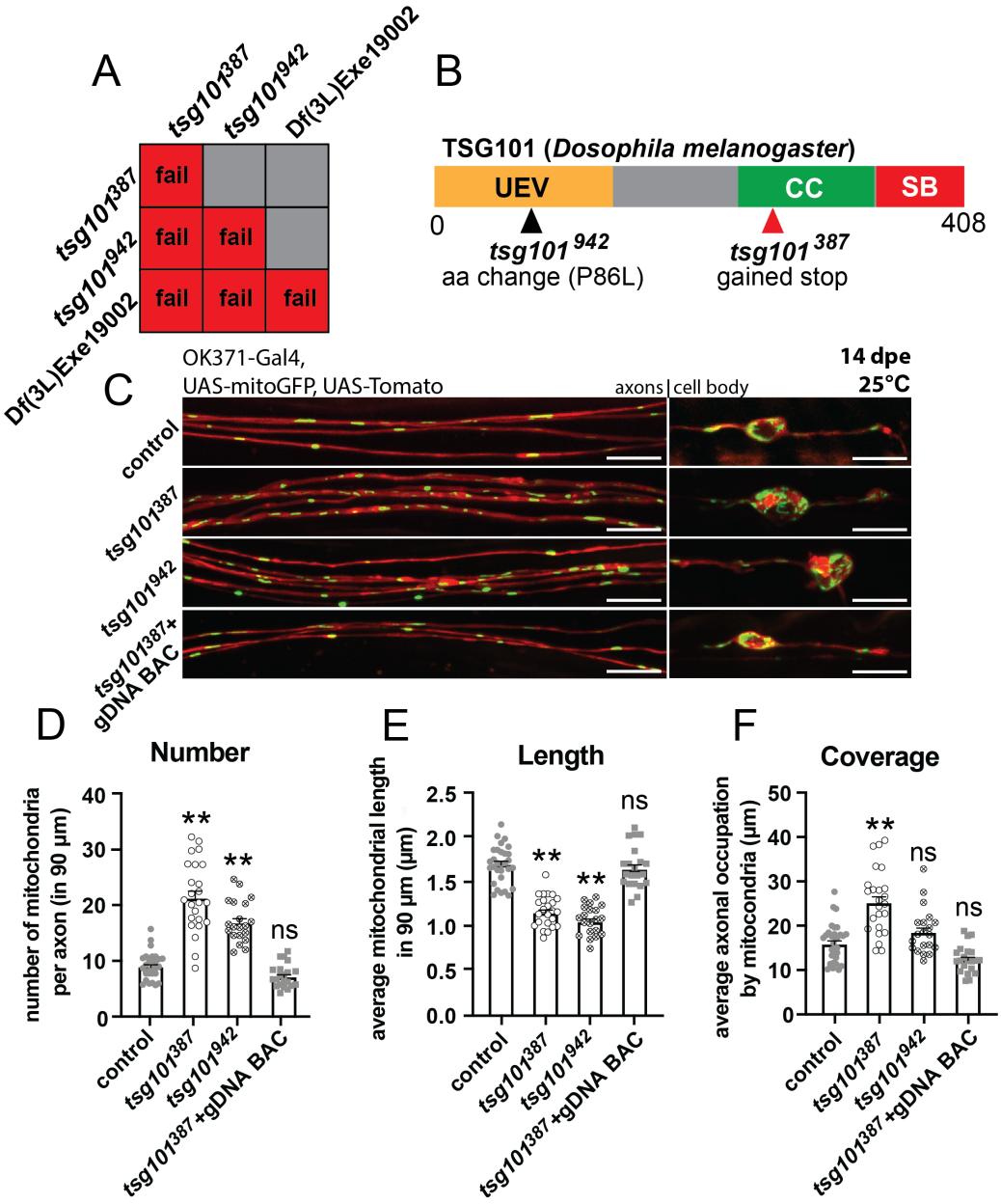

Fig. 2.2:

(A) Complementation tests were performed among two alleles of TSG101 (*tsg101*^{387} and *tsg101*^{942}) and deficiencies, or genomic deletions that uncover *tsg101* such as Df(3L)Exe19002. Other deficiencies including Df(3L)ED4674, Df(3L)ED223, Df(3L)Exe19003, Df(3L)Exe19004 were also used in the complementation tests and all failed to complement with *tsg101* mutant alleles. **(B)** A diagram of the nature of different TSG101 alleles. TSG101^{387} was the allele identified in the screen; it contains a premature stop in the coiled-coil domain (CC) (red arrowhead). TSG101^{942} is a publicly available null allele that has an amino-acid change in the Ubiquitin E2 variant domain (UEV) (black arrowhead). **(C-F)** Homozygous mutant glutamatergic neurons were generated as in the previous figure. The flies were grown at 25℃ and the cell bodies and the axons of the neurons were examined by fluorescence microscopy at 14 days post eclosion (dpe). Scale bar: 10 μm. *tsg101*^{387} exhibited elevated mitochondrial number, decreased mitochondrial size and hence increased overall axonal occupation by the mitochondria, and this phenotype could be suppressed by re-expressing TSG101 using genomic DNA BAC; *tsg101*^{942} showed a similar but slightly weaker phenotype. At least 20 wings (one wing/animal) were examined for each genotype (N≥20). Every individual data point represents one animal. All data were analyzed via one-way ANOVA. $^{**}p<0.01$. ns: not significant. Error bar: SEM.

Fig. 2.3: Age-dependent TSG101-mutant phenotypes.

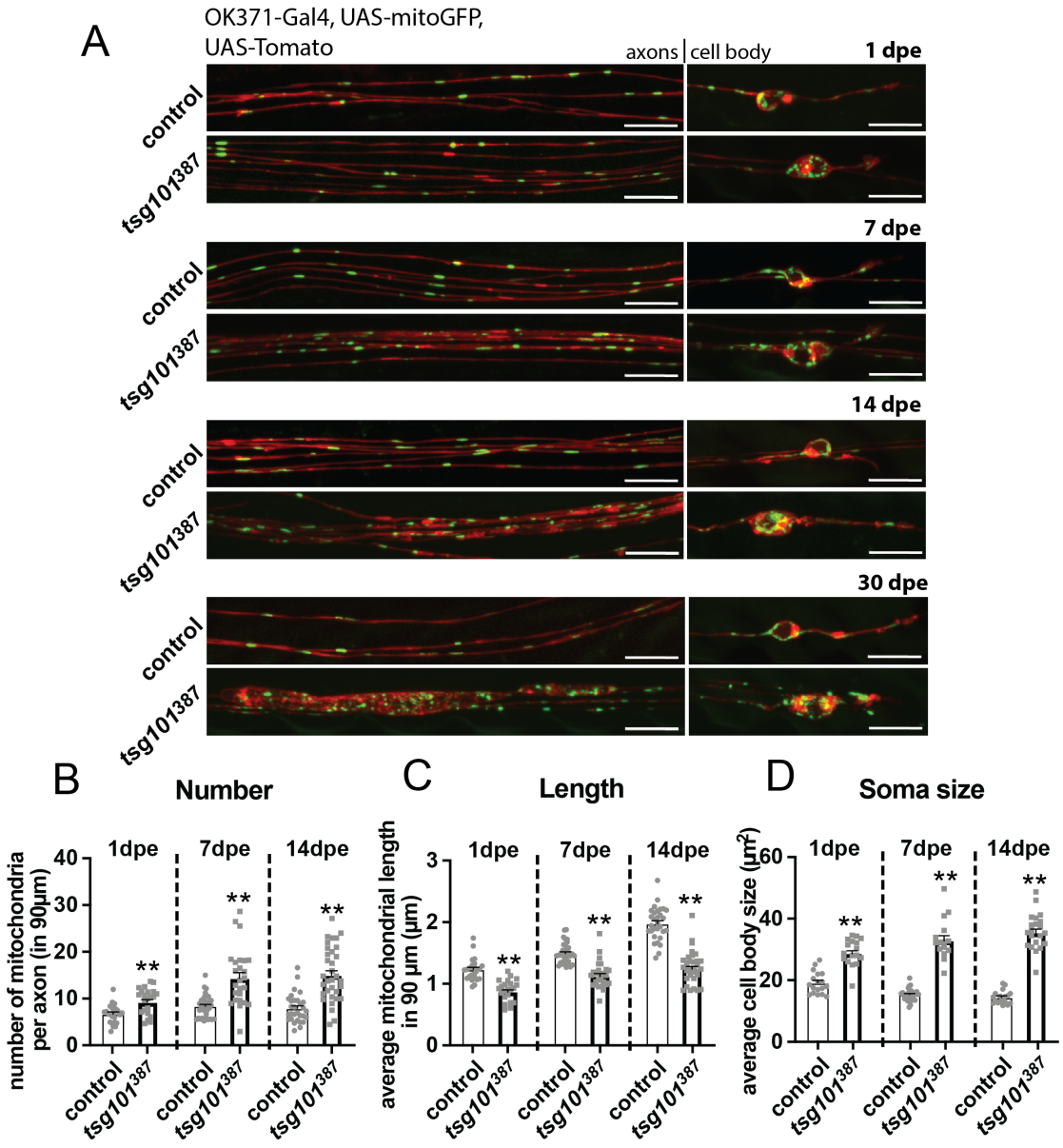

Fig. 2.3:

(A-D) Mutant neurons were generated and labeled the same way as in Fig 2.1. Axonal mitochondria (B, C) and cell body size (D) of the mutant neurons were examined and quantified at 1dpe, 7dpe and 14dpe. Mitochondria at 30 dpe were not quantified due to spontaneous neurodegeneration at 30dpe. Data within the same time point were analyzed via unpaired student t-test. At least 15 wings (one wing/animal) were examined for each genotype ($N \geq 15$). $^{**}p<0.01$. Error bar: SEM. Scale bar: 10 μm.

Fig. 2.4: The accumulation of endolysosomes and their impeded mobility in TSG101-mutant neurons

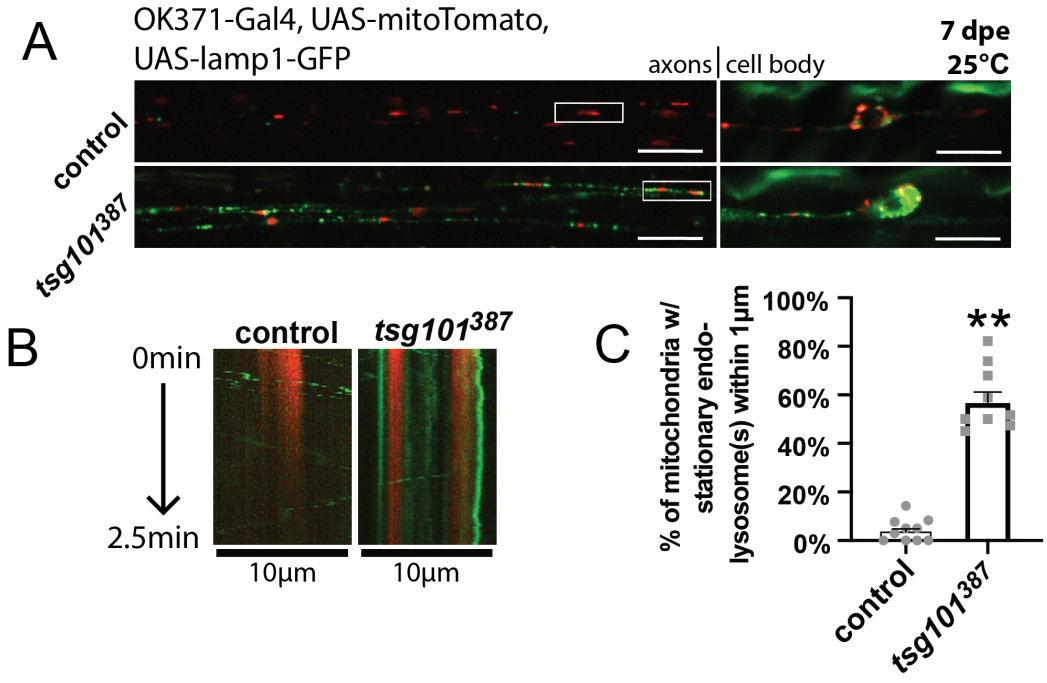

Fig. 2.4:

(A-C) The neurons were labeled, with mitochondria labeled in red and endolysosomes labeled in green (Lamp1-GFP), and live-imaged for 2.5 minutes. Single frames of the recorded videos of the neurons were shown in (A). Boxed areas were further used to make kymographs to show vesicle movements (B). Scale bar: 10 μm. The percentage of the mitochondria with stationary endolysosomes in close proximity (within 1 μm range) was calculated and shown in (C). Dozens of mitochondria were counted in each animal, with about 10 wings (one wing/animal) used in each genotype (N≅10). Data were analyzed via unpaired student t-test. $^{**}p<0.01$. Error bar: SEM.

Chapter 3: Investigating the molecular mechanisms by which TSG101 regulates axonal mitochondria—the canonical ESCRT pathway is not required for mitochondrial regulation in axons

Results

TSG101 is best known as a component of the ESCRT-I complex, one of several ESCRT complexes (ESCRT-0, ESCRT-I, ESCRT-II, ESCRT-III and the accessory ESCRT complex) that drive the functional maturation of endosomes into multi-vesicular bodies (MVBs). To initiate the canonical ESCRT pathway, ESCRT-0 recognizes ubiquitylated membrane-bound proteins and recruits ESCRT-I. The ESCRT-I recognizes ESCRT-0 and the ubiquitylated proteins; TSG101 in ESCRT-I is the most instrumental in this recognition. ESCRT-I then recruits ESCRT-II and subsequently ESCRT-III, which drives the budding of the membrane toward the inside of the endosome. The accessory ESCRT complex, as the last step, remodels ESCRT-III and scissors the membrane to form vesicles inside the endosome—hence the MVB. MVBs can either fuse with the plasma membrane to release the vesicles formed by the ESCRT machinery, a process called exocytosis, or merge with lysosomes to degrade the content inside the MVB (Jiao et al., 2009; Raiborg and Stenmark, 2009; Vaccari et al., 2009).

To determine whether other ESCRT genes also regulate axonal mitochondria, I knocked down most components of all ESCRT complexes by RNAis in the glutamatergic sensory neurons in the *Drosophila* wing. Surprisingly, none of the knockdowns phenocopied either the increased mitochondrial number or the decreased mitochondrial

length, as observed in the *tsg101* mutant, except Shrb knockdown (Table 3.1). Shrb is a homolog of *vps32*/*snf7* in the ESCRT-III complex. Knockdown of Shrb fully phenocopied mitochondrial phenotypes in *tsg101* loss-of-function mutants (Fig. 3.1A-C). However, I was unable to generate clones for analysis of adult axons, as Shrb-mutant glutamatergic neurons underwent cell death by 1 dpe. To further test the involvement of other ESCRT genes in mitochondrial regulation, I used more rigorous loss-of-function genetic methods. I generated MARCM clones using tested and published null alleles of at least one component of each major ESCRT complex, and I found that knockout of Lsn (ESCRT-II), Vps2 (ESCRT-III), or ALiX and Mop (accessory complex) also failed to recapitulate the $tsg101^{387}$ mitochondrial phenotype (Fig. 3.1D-F). Based on the evidence presented above, I concluded that TSG101 does not regulate axonal mitochondria through canonical ESCRT signaling. As little is known about non-canonical ESCRT pathways, whether TSG101 and Shrb regulate mitochondria via the same mechanism remains unclear. Based on several of my preliminary observations, my current hypothesis is that Shrb and TSG101 might work in parallel. Shrb knockout leads to cell death by 1 dpe, much earlier than the neurodegeneration at 30 dpe upon TSG101 knockout, suggesting that Shrb might be involved in maintaining neuronal health more than TSG101. Moreover, knockdown of Shrb in TSG101-mutant background led to axon degeneration faster than in either TSG101-knockout or Shrb-knockdown background alone (Fig. 3.1A), an additive effect that suggests that TSG101 and Shrb might be genetically parallel. More rigorous experiments are needed to support this hypothesis. Meanwhile, how TSG101 or Shrb functions non-canonically remains an interesting topic to be studied.

Material & Methods

Drosophila *strains*

The following null mutant alleles and commercially available RNAi lines were used in the knockout or knockdown experiments for interrogation of the canonical ESCRT pathway:, lsn^{ss6} (BDSC:39631), $vps2^{pp6}$ (BDSC:39630), $alix^{LL05494}$ (Kyoto:140993), $shrb^{G5}$ (BDSC:39635), $shrb^{O3}$ (BDSC:39623), mop^{T612} (BDSC:63117), *5xUAS-tsg101*^{RNAi} (BDSC:35710), *5xUAS-shrb*^{RNAi} (BDSC:38305), *5xUAS-stam*^{RNAi} (BDSC:27487, BDSC:35016, VDRC:22497, VDRC:330248), *5xUAS-hrs*^{RNAi} (BDSC:28026, BDSC:33900, BDSC:34086, VDRC:330597), *5xUAS-vps37*^{RNAi} (BDSC:38304, VDRC:39885, VDRC:104530, BDSC:44010, BDSC:60416, VDRC:330553), *5xUAS-vps28*^{RNAi} (VDRC:31894, VDRC:31895), *5xUAS-vps36*^{RNAi} (BDSC:38286, VDRC:16846, VDRC:16847, VDRC:107417), *5xUAS-lsn*^{RNAi} (BDSC:38289, VDRC:21658, VDRC:110350), *5xUAS-vps25*^{RNAi} (BDSC:26286, BDSC:54831, VDRC:38821, VDRC:108105), *5xUAS-vps20*^{RNAi} (BDSC:40894, VDRC:26387, VDRC:26388, VDRC:103944), *5xUAS-vps20*^{RNAi} (BDSC:40894, VDRC:26387, VDRC:26388, VDRC:103944), *5xUAS-vps2*^{RNAi} (BDSC:38995, VDRC:24869), *5xUAS-vps4*^{RNAi} (BDSC:31751, VDRC:35125, VDRC:35126, VDRC:105977), *5xUAS-Chmp1*^{RNAi} (BDSC:28906, BDSC:33928, VDRC:1788), *5xUAS-alix*^{RNAi} (BDSC:33417, BDSC:50904, VDRC:32047, VDRC:32049), *5xUAS-usp8*^{RNAi} (BDSC:38982, BDSC:39022, VDRC:330131), and *5xUAS-mop*^{RNAi} (BDSC:28522, BDSC:32916, BDSC:34085, VDRC:14173, VDRC:104860). Flies used for MARCM clone generation were: *OK371-Gal4* (BDSC:26160), *10xUAS-IVS-myr::td-Tomato* (BDSC:32222), *5xUAS-mito::EGFP* (BDSC:8442), *asense-FLP2e* (lab stock); *tub-Gal80* (BDSC:5190, BDSC:5135,

BDSC:5132, BDSC:5191), (BDSC:1997), *FRT82B* (BDSC:2035), *FRT19A* (BDSC:1709), and *FRT80B* (BDSC:1988).

Microscopy and data analysis

Images were acquired from a Zeiss spinning disc confocal microscope with its proprietary Zen Blue software. Image processing was done with Zen Blue and Fiji. Fiji was used to quantify mitochondrial number and length. All statistical analyses were conducted by using Graph Pad Prism 8. Data in Fig 3.1 were analyzed via one-way ANOVA, with at least 30 wings (one wing/animal) checked in each genotype in (A-C) ($N \geq 30$) and at least 20 wings (one wing/animal) examined per genotype in (D-F) ($N \geq 20$).

Figures & Tables

Table 3.1: Recapitulation of TSG101-mutant phenotype by knockdown (KD) or knockout (KO) of ESCRT components.

Gene Name	ESCRT complex	KD phenocopy?	KO phenocopy?
stam	0	No	N/D
vps27/hrs	0	No	N/D
tsg101/ept	I	Yes	Yes
vps37	I	No	N/D
vps28	I	No	N/D
vps36	II	No	N/D
vps22/lsn	II	No	No
vps25	II	No	N/D
vps20	III	No	N/D
vps32/shrb	III	Yes	N/D*
vps2	III	No	No
vps4	Accessory	No	N/D
Chmp1	Accessory	No	N/D
alix	Accessory	No	No
usp8/ubpy	Accessory	No**	N/D
mop	Accessory	No	No***

Table 3.1:

Multiple RNAis were used for each gene to knockdown genes of interest (see in Materials & Methods). Reported null alleles were selected and used in knockout experiments to recapitulate TSG101-mutant phenotypes (detailed results shown in Fig. 3.1). Multiple genes were tested in each of the five complexes (ESCRT-0, ESCRT-I, ESCRT-II, ESCRT-III and ESCRT-accessory). Successful phenocopy indicates recapitulation of both neuronal (increased cell body size) and mitochondrial (both increased number and decreased size) phenotypes. *early neurodegeneration; **only mitochondrial size was recapitulated; ***only neuronal blebbing phenotype was occasionally recapitulated.

Fig. 3.1: TSG101 functions as a novel regulator of axonal mitochondria in a non-canonical, ESCRT-independent manner.

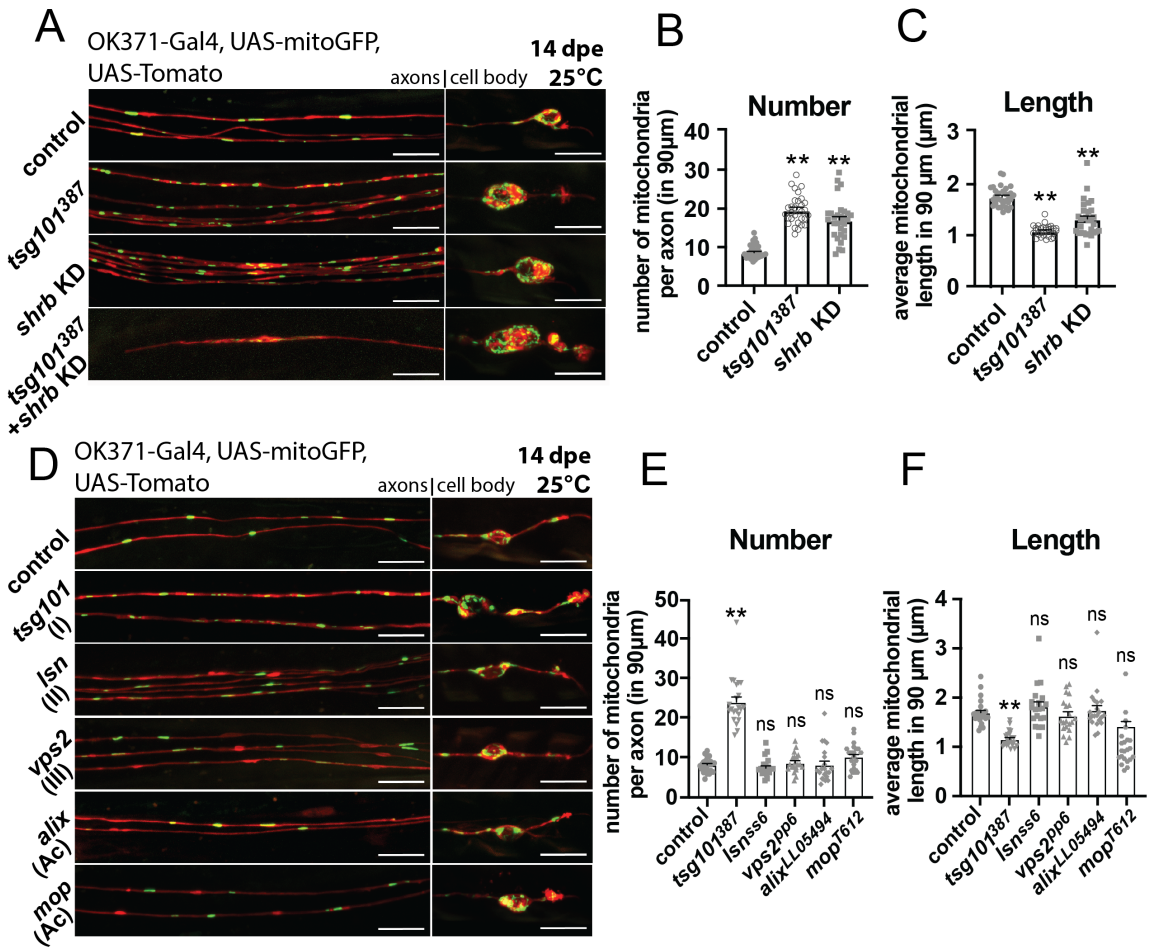

Fig. 3.1:

All neurons were generated and labeled as in Fig. 2.2. **(A-C)** Knockdown of Shrb (*shrb* KD, RNAi line BDSC:38305) of the ESCRT-III showed *tsg101*-mutant-like phenotype. However, knockdown of Shrb in *tsg101*-null conditions caused axon die-back, therefore no quantification of axonal mitochondria was conducted. At least 30 wings (one wing/animal) were examined in each genotype (N≥30). **(D)** Null alleles of each gene in different ESCRT complexes were selected to generate homozygous mutant clones in *Drosophila* wings: $tsg101^{387}$ in the ESCRT-I (I), lsn^{ss6} in the ESCRT-II (II), $vps2^{pp6}$ in the ESCRT-III (III), and $alix^{LL05494}$ and mop^{T612} in the Accessory complex (Ac). Mitochondrial number and length were analyzed and quantified in (E) and (F), respectively. At least 20 wings (one wing/animal) were examined in each genotype (N≥20). All data were analyzed via one-way ANOVA. $^{**}p<0.01$. Error bar: SEM. Scale bar: 10 μm.

Chapter 4: Investigating the molecular mechanisms by which TSG101 regulates axonal mitochondria—PINK1/Parkin-mediated mitophagy and macroautophagy are dispensable in axons for mitochondrial regulation

Results

Recent work has identified a link between the ESCRT machinery and mitochondrial clearance. CHMP2A/Vps2 in ESCRT-III is required during mitophagy for phagophore closure to form functional autophagosomes (Takahashi et al., 2018; Zhen et al., 2019). Snf8/Lsn in ESCRT-II and TSG101 in ESCRT-I are involved in autophagy-independent but Parkin-dependent mitochondrial clearance (Hammerling et al., 2017). Therefore, I reasoned that the increase in mitochondrial number in axons I observed might be the result of failed mitochondrial clearance. I first checked whether mitochondrial clearance was deterred upon TSG101 abolition by using a well-established genetic tool, mito-QC, which allows for visualization of mitochondrial clearance using a pH-sensitive fluorophore that alters fluorescence upon mitochondrial entry into acidic vesicles during degradation (Fig. 4.1A) (Lee et al., 2018; McWilliams et al., 2016). In control axons and the cell body, I detected both normal (yellow) mitochondria and mito-lysosomes (red), which represent mitochondria undergoing lysosomal degradation, but I observed an absence of mito-lysosomes in TSG101 mutants, indicating that mitochondrial turnover is largely attenuated (Fig. 4.1B). As live-cell imaging in Fig 2.4 showed more stationary endolysosomes

juxtaposing with mitochondria, the loss of mitochondrial turnover may occur due to defects in endolysosomal trafficking.

I reasoned that TSG101 might be upstream of the mitophagy pathway, in which Parkin and/or PINK1 may be involved, to turn over axonal mitochondria; a recent study also showed, in a non-neuronal *in vitro* setting, that TSG101 plays a role in mitochondrial clearance that is independent of autophagy but dependent on Parkin (Hammerling et al., 2017). I thus first checked whether Parkin and PINK1 were involved in axonal mitochondrial turnover by over-expressing PINK1 or Parkin, key components for mitophagy. However, not only did it fail to rescue TSG101-mutant phenotype, but over-expressing Parkin even caused neurodegeneration (Fig. 4.1C), suggesting that either mitophagy was not active in this context or that it was required only at low levels. I further blocked mitophagy by knocking out Parkin or PINK1 to recapitulate TSG101-mutant phenotype. I found, surprisingly, that neither mutant exerted significant effects on axonal mitochondrial numbers or size, nor on axon maintenance (Fig. 4.1D-F), suggesting that Parkin/PINK1-dependent mitochondrial turnover is dispensable in axons.

Since the TSG101-mutant phenotype cannot be explained by the lack of Parkin or PINK1, and emerging evidence has shown that basal mitophagy can be Parkin- and PINK1-independent (Lee et al., 2018; McWilliams et al., 2018), I tried more extreme means—impeding the entire autophagy process by knocking out *atg6* (Beclin-1 homolog) or over-expressing dominant-negative *atg1* (ULK1 homolog)—to block both mitophagy and macro-autophagy. Neither alteration in mitochondrial number nor the size was seen in these cases (Fig. 4.2A-C); however, I did find that the cell bodies drastically increased in size (Fig. 4.2D). Moreover, somal mitochondria changed from linear shapes to more globular

ones (reflected in lower aspect ratio in *tsg101*^{387} mutants, Fig. 4.2E), and the mitochondrial mass significantly increased (Fig. 4.2F), although the increase was proportionate to that in cell body size, leading to no change in overall mitochondrial coverage (Fig. 4.2G). This phenotype persisted up to 30 dpe, where the cell body phenotype progressively worsened, and yet the axonal mitochondria stayed morphologically similar to wildtype, with occasional blebs present (Fig. 4.2H). As I confirmed that mitochondria no longer go through lysosomal degradation when autophagy is genetically blocked (Fig. 4.2I, J), I conclude that axonal mitochondrial populations can be maintained at normal levels even without PINK1, Parkin, or autophagy. This suggests that the TSG101-mediated, autophagy-independent but Parkin-dependent mitochondrial clearance reported previously is mechanistically distinct from TSG101-mediated mitochondrial clearance in axons. Furthermore, these findings support the premise that mitochondrial clearance mechanisms are compartmentalized in neurons, since we observe changes in mitochondria in cell bodies with manipulation of autophagy, but not in axons. While the detailed mechanism by which neurons turn over axonal mitochondria remains to be explored, I conclude that the TSG101-mutant mitochondrial phenotype is not caused by lack of classical mitophagy or autophagy.

Material & Methods

Drosophila *strains*

The *UAS-mito-QC* fly for visualizing mitochondrial turnover events (*i.e.*, mito-lysosomes) was a gift from the Whitworth Lab at the University of Cambridge, UK (Lee et al., 2018). The following flies were used for investigating the role of PINK1/Parkin-

mediated mitophagy and autophagy in axonal mitochondrial maintenance: *parkin*$^{\Delta 21}$ (BDSC:51652), *pink1*^{5} (BDSC:51649), *UAS-pink1* (BDSC:51648), *UAS-parkin* (BDSC:51651) *atg6*$^{\Delta 1}$ (Zhao et al., 2018) and *UAS-atg1.K38Q* (dominant negative; (Berry and Baehrecke, 2007)). The flies used for MARCM clone induction were *OK371-Gal4* (BDSC:26160), *10xUAS-IVS-myr::td-Tomato* (BDSC:32222), *5xUAS-mito::EGFP* (BDSC:8442), *asense-FLP2e* (lab stock); *tub-Gal80* (BDSC:5190, BDSC:5135), *FRT2A* (BDSC:1997), and *FRT82B* (BDSC:2035).

Microscopy and data analysis

Images were acquired from a Zeiss spinning disc confocal microscope along with its proprietary Zen Blue software. Image processing was done with Zen Blue and Fiji. Fiji was used to quantified mitochondrial number, mitochondrial length, somal mitochondrial size and shape, and cell body size. All statistical analyses were conducted by using Graph Pad Prism 8. Data in Fig 4.1A-B were analyzed via unpaired student t-test, with 10 wings (one wing/animal) checked; Fig4.1D-F were analyzed by using 2-way ANOVA, with at least 20 animals examined ($N \geq 20$). At least 20 wings (one wing/animal) were imaged in in Fig. 4.2A-G, with data in Fig. 4.2B-C analyzed by one-way ANOVA and in Fig. 4.2D-G analyzed via unpaired student t-test. Data in Fig4.2I-J were generated using at least 14 wings (one wing/animal) in each genotype, and analyzed using unpaired student t-test as well.

Figures

Fig. 4.1: Blocking Parkin/PINK1-mediated mitophagy in neurons did not recapitulate the axonal mitochondrial phenotype of TSG101 mutants.

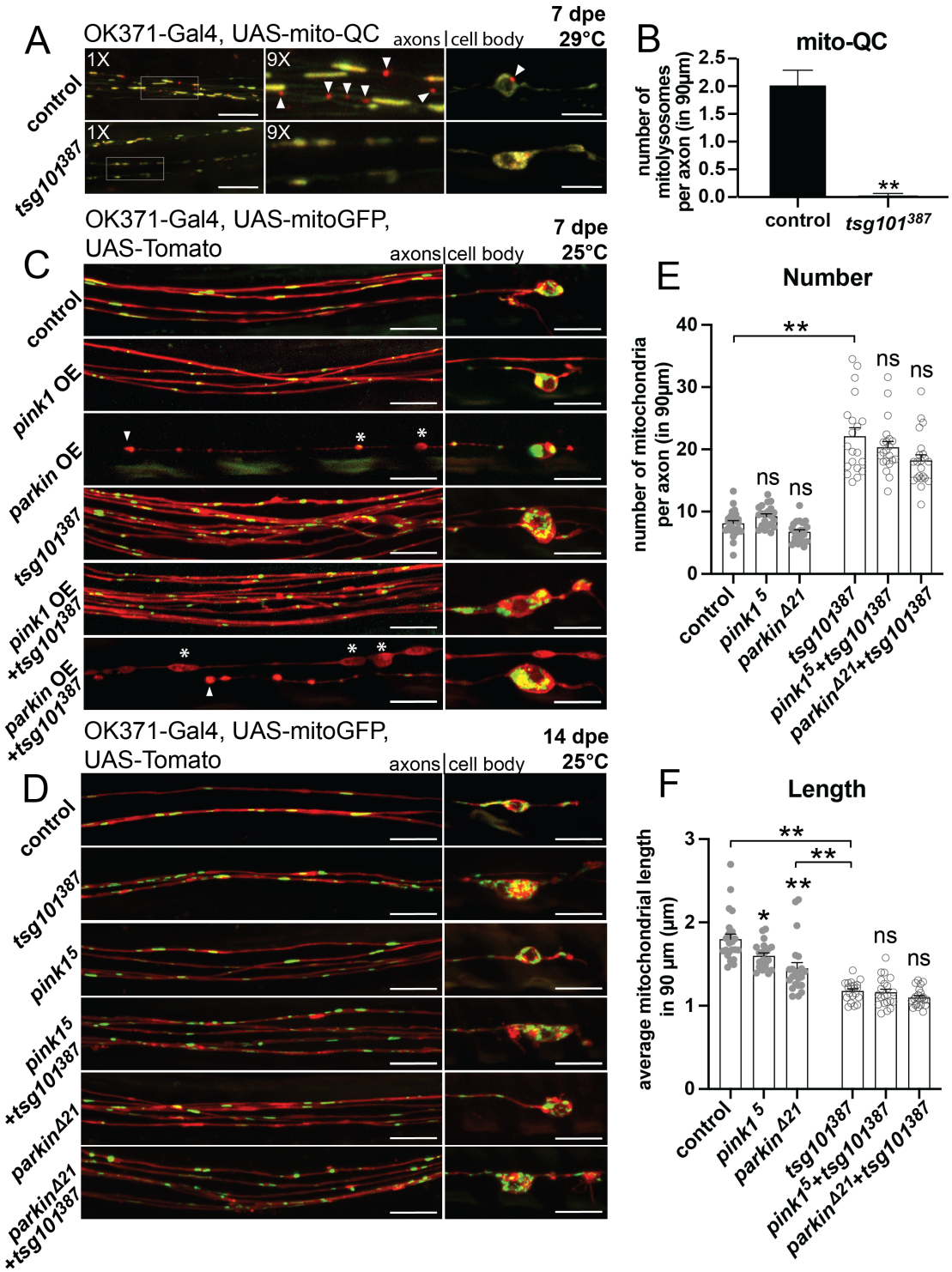

Fig. 4.1:

(A, B) mito-QC was utilized to visualize mitochondrial turnover events: normal mitochondria in yellow (green + red) and lysosome-associated mitochondria in red (mito-lysosomes, indicated by white arrowheads). Flies were grown in 29°C and checked at 7 dpe. The number of mito-lysosomes per axon in (A) was quantified and shown in (B), analyzed by unpaired t-test. 10 wings (one wing/animal) were examined for each genotype (N=10). **(C)** PINK1 or Parkin was over-expressed to activate mitophagy in an attempt to rescue the TSG101-mutant phenotype. However, over-expressing PINK1 shrunk mitochondrial size, and over-expressing Parkin led to neurodegeneration (axon stumps pointed by white arrowheads; blebs indicated by asterisks). Flies were raised in 25°C and the neurons were checked at 7 dpe. **(D-F)** Homozygous mutant neurons were sparsely generated and labeled red and mitochondria in green. Null alleles of PINK1 (*pink1*^{5}) and Parkin (*parkin*$^{\Delta 21}$) were used to suppress mitophagy. Flies were grown in 25°C and checked at 14 dpe. Mitochondria were subsequently quantified and analyzed in (E) and (F). At least 20 wings (one wing/animal) were examined in each genotype (N≥20). Data were analyzed via two-way ANOVA. *p<0.05. **p<0.01. Error bar: SEM. Scale bar: 10 μm.

Fig. 4.2: Blockade of autophagy led to phenotypes in the cell body but exerted no effect on axonal mitochondrial morphology.

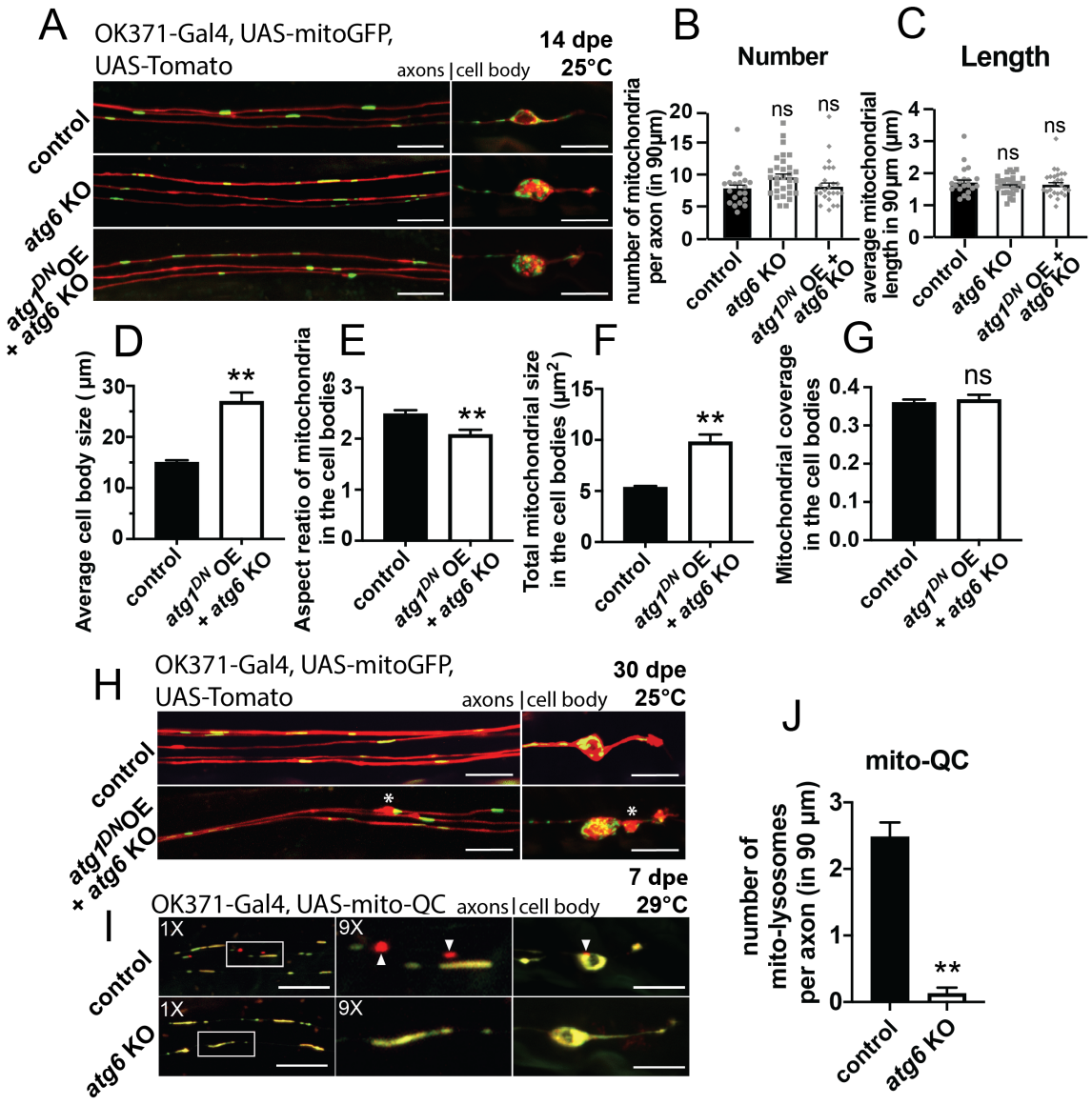

Fig. 4.2:

(A-C) Blocking autophagy by knocking out *atg6* (Beclin-1) or over-expressing dominant-negative *atg1* (ULK1) or both. Flies were grown in 25℃ and checked at 14 dpe. Quantification of axonal mitochondria is shown in (B) and (C), analyzed via one-way ANOVA. **(D-G)** blocking autophagy also led to an increase in soma size (D), and somal mitochondria changed shape (E) and increased in mass (F), although total mitochondrial coverage remained unchanged (G). The same batch of flies used in (A) was used here for cell body quantification. All data were analyzed via unpaired t-test. At least 20 wings (one wing/animal) were checked in each genotype ($N \geq 20$). **(H)** At 30 dpe, although autophagy was blocked in the same way as in (A), axonal mitochondria remained morphologically intact. While most of the time the axons were intact, with occasional blebs visible (indicated by asterisks), the cell bodies and dendrites were always defective, similar to the cell bodies in TSG101 mutants. **(I, J)** mito-QC (also used in Fig. 4.1A) was utilized to visualize mitophagy events when autophagy was genetically blocked (*atg6* knockout). About 2.5 mitochondria were observed to undergo mitophagy (visualized by the presence of mito-lysosomes, indicated by white arrowheads), whereas nearly no mito-lysosomes were detected in *atg6*-knockout axons, suggesting mitophagy is attenuated upon autophagy blockade. Quantification is shown in (J). Data were analyzed via unpaired student t-test. At least 14 wings (one wing/animal) were checked in each genotype ($N \geq 14$). $^{**}p<0.01$. Error bar: SEM. Scale bar: 10 μm.

Chapter 5: Investigating the molecular mechanisms by which TSG101 regulates axonal mitochondria—mitochondrial biogenesis is altered in TSG101mutants

Results

Although I ruled out mitophagy and macroautophagy as the pathways that turn over axonal mitochondria, I have not yet addressed the possibility that TSG101 may be involved in other types of mitochondrial clearance, such as a type of MDV that does not require Parkin, PINK1, or autophagy. However, our current understanding of MDVs is superficial, and thus the means to manipulate them are limited. If TS101 is involved in mitochondrial turnover, I would predict that TSG101-mutant neurons would accumulate dysfunctional mitochondria and potentially have decreased ATP levels. To explore this possibility, I utilized two different roGFP genetic tools (GSSG-sensing and H_2O_2-sensing) to measure redox potential in mitochondria, which is an indicator of overall mitochondrial health—an increased oxidation state increases the 405 nm/488 nm ratio, and it correlates well with increased mitochondrial damage and dysfunction (Albrecht et al., 2011). Intriguingly, mitochondria in TSG101-mutant axons were less oxidized than controls, indicating the mitochondria were, in contrast to my prediction, healthier than controls. As a further control for the reliability of the sensor, human mitochondrial uncoupling protein (hUCP2) was over-expressed to artificially render mitochondria more oxidized, and a >50% increase in the 405 nm/488 nm ratio was observed (Fig. 5.1A-D). Moreover, by utilizing an ATP-sensing GFP ATPsnFR (developed by Lobas et al., 2019), I found that neurons lacking

TSG101 had a significant increase in cytoplasmic ATP levels, and this increase was abolished when ATP synthesis by OXPHOS was discharged by over-expressing hUCP2 (Fig. 5.1E, F). These data suggest that the mitochondrial phenotype caused by loss of TSG101 may instead be due to activated mitochondrial biogenesis.

Highly functional mitochondria require constant protein provision from the nuclear genome, and the master transcription co-activator PGC-1α and its interacting transcription factors, such as Nrf2, are responsible for activating nuclear-encoded mitochondrial gene expression. To investigate whether the highly functional mitochondria in TSG101mutants were the result of activated mitochondrial biogenesis, we knocked down *srl* (PGC-1α homolog) and *cnc* (Nrf2 homolog) in both wild-type and TSG101-mutant neurons. With two different RNAi lines for each gene, knockdown of Srl or Cnc led to smaller mitochondrial size and normal mitochondrial number, resulting in a decrease in overall mitochondrial content, which is expected after blocking mitochondrial biogenesis. When *srl* or *cnc* were knocked down in TSG101 mutants, the mitochondrial phenotype was successfully rescued, suggesting that the increase in mitochondrial number and the decrease in mitochondrial size in TSG101-mutant axons require mitochondrial biogenesis mediated by PGC-1α and Nrf2 (Fig. 5.2).

TFEB is a positive regulator of PGC-1α in the context of nutrient deprivation and exercise (Mansueto et al., 2017; Settembre et al., 2013). Therefore, I investigated the role of TFEB as a potential link between TSG101 and PGC-1α. Knockdown of Mitf (the mammalian homolog of TFEB) with two different RNAi lines rescued the TSG101-mutant mitochondrial phenotype (Fig. 5.3A-C), suggesting that TFEB is also downstream of TSG101 in controlling mitochondrial biogenesis.

The mTOR pathway is also a modulator of mitochondrial biogenesis (Cunningham et al., 2007; Dominy and Puigserver, 2013) and can control TFEB activation (Martina et al., 2012; Napolitano et al., 2018). The mTOR inhibitor Tsc1 was also uncovered in our forward genetic screen (see Chapter 2). In addition, loss of Tsc1 has been found to activate mitochondrial biogenesis (Chen et al., 2008). I therefore explored the epistatic relationship between Tsc1 and TSG101. When Tsc1 was knocked down in wild-type clones, mitochondrial numbers were significantly increased, even higher than in TSG101 mutants alone, yet no difference in mitochondrial size was detected (Fig. 5.3D-F). Knockdown of Tsc1 in TSG101 null clones had no additive effect on the number of mitochondria in axons (Fig. 5.3E). This finding suggests that TSG101 controls mitochondrial biogenesis in an mTOR-independent manner, or at least not through Tsc1. This result also complements the previous findings that the mTOR pathway regulates mitochondrial biogenesis via activating a different transcription factor, YY1, rather than Nrf2 (Cunningham et al., 2007; Dominy and Puigserver, 2013), further supporting the notion that TSG101 and the mTOR pathway are parallel to each other in mitochondrial regulation. Our model suggests that TSG101 and mTOR function in parallel pathways that converge on TFEB to regulate mitochondrial biogenesis (Fig. 5.3G).

To further investigate how TSG101 controls TFEB, I hypothesized that TFEB-dependent mitochondrial biogenesis may be triggered by nutrient deprivation, as has been previously reported (Settembre et al., 2013). I explored this possibility by feeding the flies with scarce media (see Materials & Methods) from 1 dpe to trigger a nutrient deprivation response, in an attempt to recapitulate TSG101-dependent mitochondrial biogenesis. However, when imaged at 14 dpe, whole animal starvation did not lead to an increase in

mitochondrial number as expected; it instead shortened mitochondrial sizes in both the control and TSG101 mutants (Fig. 5.4A-C), leading to decreases in overall mitochondrial content in both genotypes. The starved flies started dying after 14 dpe, therefore no data from later time points were collected. Though preliminary, this finding suggested that starvation response was unlikely the upstream factor that activates TFEB in TSG101-mutant axons. How TFEB is activated in a TSG101-dependednt manner remains to be determined.

Lastly, new mitochondria are generated by fission from the existing ones, which can be achieved by activating fission or inhibiting fusion. I thus first checked whether mitochondrial biogenesis required activated mitochondrial fission. I blocked fission by knocking out a critical fission gene, *drp1*, and that rescued both the mitochondrial number and size in axons caused by TSG101 knockdown, supporting the notion that mitochondrial fission is downstream of TSG101 as a final step to complete mitochondrial biogenesis (Fig. 5.5A-C). I also checked the effect of mitochondrial fusion by knocking down an essential fusion gene, *marf,* to recapitulate the mutant phenotype. Knockdown of Marf in control clones successfully decreased mitochondrial length to levels indistinguishable from $tsg101^{387}$ mutants at 7 dpe, yet had no effect on number (Fig. 5.5D-F). To our surprise, *marf* knockdown rescued mitochondrial number in TSG101mutant axons to near control levels (Fig. 5.5E). We further investigated the effect of *marf* knockdown at the earliest time point, 1 dpe, where the mitochondrial phenotype was not fully manifested, and found that *marf* knockdown had little effect (Fig. 5.5G-I). This finding suggests that the age-dependent increase of mitochondrial number from 1 to 7 days requires Marf and that fusion is a necessary initial step for biogenesis.

Material & Methods

Drosophila *strains*

The redox-sensing GFP (roGFP) transgenic flies used for assessing mitochondrial health were: *5xUAS-mito-Grx1-rorGFP2* (GSSG-sensing; BDSC:67664) and *5xUAS-mito-roGFP2-Orp1* (H_2O_2-sensing; BDSC:67667). The *UAS-ATPsnFR* transgenic fly was made in this lab with the plasmid provided by the Looger Lab at the Janelia Research Campus. The following over-expression constructs, RNAi lines and the mutant allele were used for epistatic analyses or general experiments: *UAS-hUCP2* (Fridell et al., 2005), *5xUAS-tsg101^{RNAi}* (BDSC:35710), *5xUAS-Tsc1^{RNAi}* (BDSC:54034), *5xUAS-marf^{RNAi}* (BDSC:55189), *5xUAS-srl^{RNAi}* (VDRC:330271), *5xUAS-srl^{RNAi}* (VDRC:103355), *5xUAS-cnc^{RNAi}* (BDSC:40854), *5xUAS-cnc^{RNAi}* (VDRC:37673), *5xUAS-Mitf^{RNAi}* (BDSC:44561), *5xUAS-Mitf^{RNAi}* (VDRC:109184), and *drp1^{1}* (BDSC:24885). Flies used for MARCM clone induction were *OK371-Gal4* (BDSC:26160), *nSyb-Gal4* (BDSC:51635), *10xUAS-IVS-myr::td-Tomato* (BDSC:32222, BDSC:32221), *5xUAS-mito::EGFP* (BDSC:8442, BDSC:8443), *5xUAS-mito::td-Tomato* (lab stock, Smith et al., 2019), *asense-FLP2e* (lab stock), *asense-FLP3b* (lab stock), *tub-Gal80* (BDSC:5190, BDSC:5192), *FRT2A* (BDSC:1997), *FRT82B* (BDSC:2035) *FRT40A* (BDSC:1646), and *FRTG13* (BDSC:1956).

Whole-animal starvation

To induce a starvation response, *Drosophila* adults were deprived of nutrients for the entire 14-day adulthood. Animals were raised in standard cornmeal media until the pupal stage. Pupae were transferred to vials with scarce media composed of 4% (w/v)

sucrose (Fisher Bioreagents), 1.5% (w/v) agar (Fisher Bioreagents) and 0.5% (w/v) propionic acid (Sigma-Aldrich). The eclosed adults were kept in the vials with scarce media until being checked with fluorescence microscopy at 14 dpe.

Microscopy and image analysis

Images were acquired from a Zeiss spinning disc confocal microscope along with its proprietary Zen Blue software. Image processing was done with Zen Blue and Fiji. Fiji was used to quantify fluorescence intensities and mitochondrial number and length. All statistical analyses were conducted by using Graph Pad Prism 8. Data in Fig. 5.1A-D were analyzed via unpaired t-test, with at least 10 wings (one wing/animal) checked in each genotype ($N \geq 10$). At least 14 wings (one wing/animal) were examined in each genotype in Fig. 5.1E-F, and the data were analyzed via two-way ANOVA. Data in Fig. 5.2 and 5.3 were obtained from examining at least 30 wings per genotype (one wing/animal, $N \geq 30$) and analyzed via two-way ANOVA. Data in the rest of the figures were also analyzed using two-way ANOVA, with at least 20 wings ($N \geq 20$) in Fig. 5.4 and about 20 wings (one wing/animal, $N \cong 20$) in Fig. 5.5 were checked in each genotype.

Figures

Fig. 5.1: Mitochondria in TSG101 mutants were less oxidized and generated more ATP compared to controls.

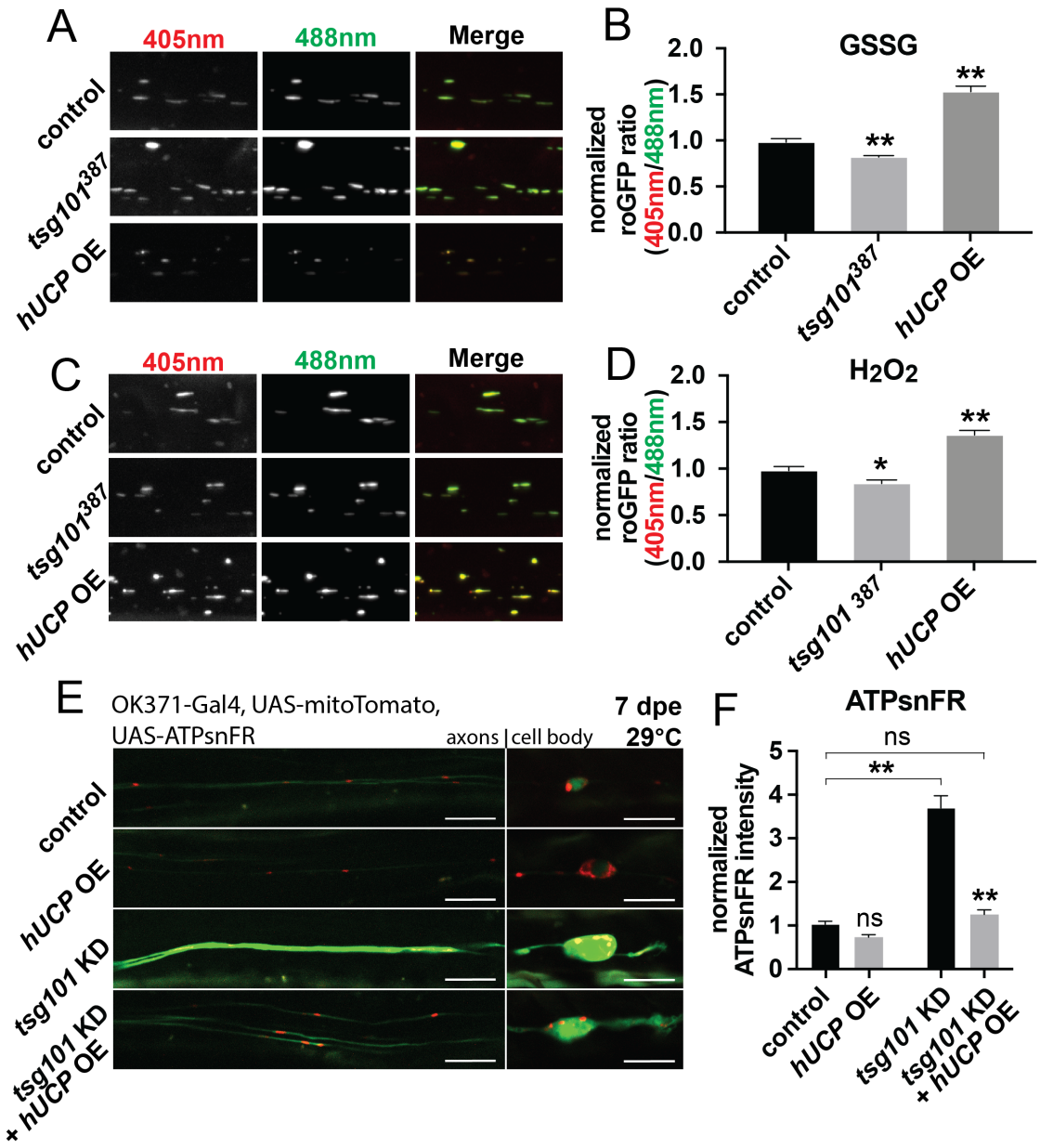

Fig. 5.1:

(A-D) Redox-sensing GFPs (roGFPs) were utilized and expressed in mitochondria to reactive oxygen species. Fluorescence intensities were measured with 405 nm (pseudo-colored red) and 488 nm (pseudo-colored green) laser excitations. roGFP ratios were determined by the measured fluorescence intensity from 405 nm divided by that from 488 nm. 405 nm/488 nm ratios were normalized to controls. A higher ratio indicates a more oxidized mitochondrion. Over-expression of human mitochondrial uncoupling protein (hUCP2) was used to make mitochondria more oxidized by disrupting mitochondrial membrane potential to ascertain the reliability of the sensors. Flies were grown in 25°C and checked at 14 dpe. Data were analyzed via unpaired t-test. At least 10 wings (one wing/animal were examined in each genotype ($N \geq 10$). Error bar: SEM. $*p<0.05$. $**p<0.01$.

(E-F) ATP-sensing GFP (ATPsnFR, green) was expressed in the cytosol to measure cytosolic ATP levels. ATPsnFR intensities were normalized to the fluorescence intensity of mitochondria (mito::td-Tomomato, red), and the normalized ATPsnFR intensities were then normalized again to that of controls. Flies were raised at 29°C and examined at 7 dpe. At least 14 wings (one wing/animal) were examined in each genotype ($N \geq 14$). Data were analyzed via two-way ANOVA. Error bar: SEM. Scale bar: 10 μm. $**p<0.01$.

Fig. 5.2: Loss of TSG101 activates PGC-1α (*srl*)/Nrf2 (*cnc*)-dependent mitochondrial biogenesis.

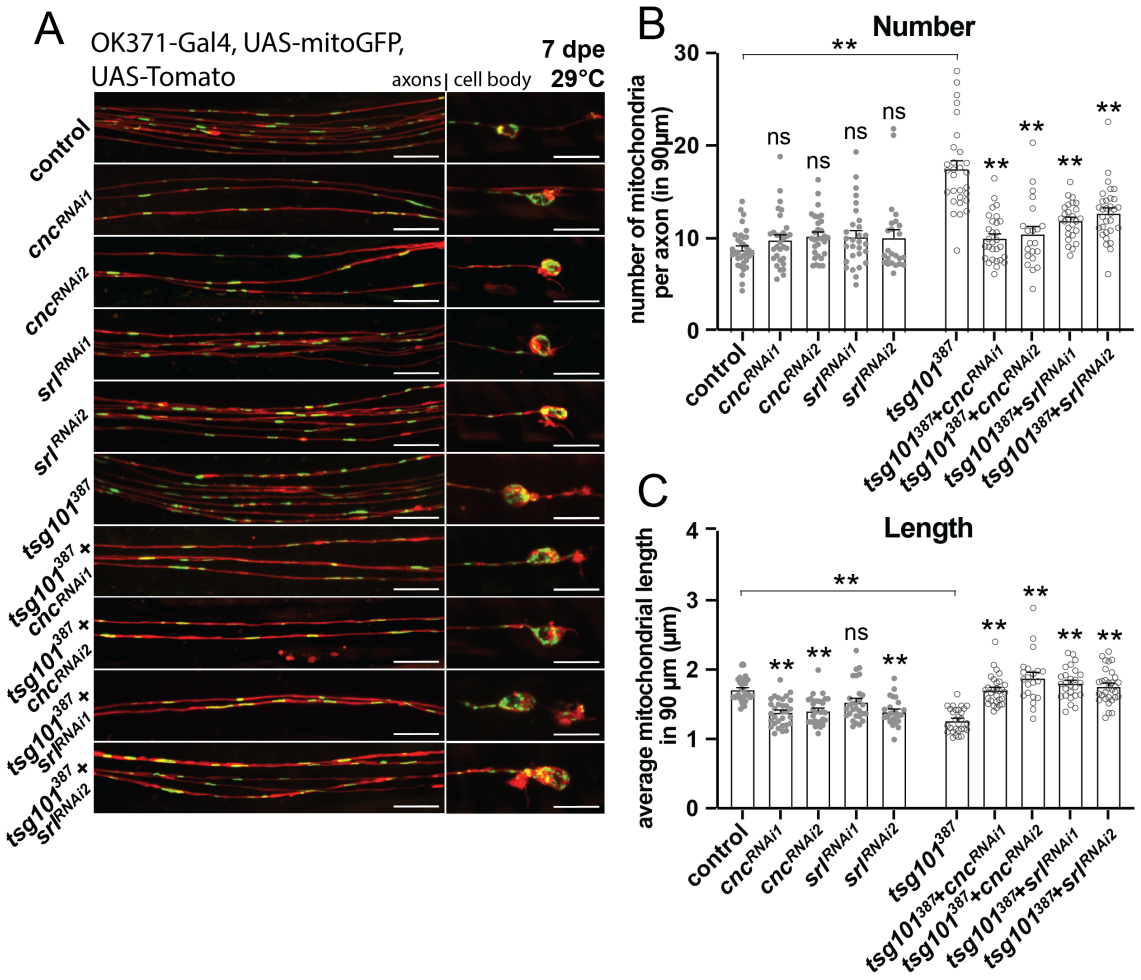

Fig. 5.2:

(A-C) Homozygous mutant neurons were generated and labeled using the same approach as in Chapter 4. Two independent RNAis were used to knock down PGC-1α (*srl*) or Nrf2 (*cnc*). All four independent RNAis were able to successfully rescue the mitochondrial phenotype resulting from TSG101 ablation. Quantification of number and length are shown in (B) and (C) respectively. At least 30 wings (one wing/animal) were examined in each genotype (N≥30). Data were analyzed via two-way ANOVA. Error bar: SEM. $^{**}p<0.01$. Scale bar: 10 μm.

Fig. 5.3: TSG101-dependent mitochondrial regulation is dependent on TFEB and independent of the mTOR pathway

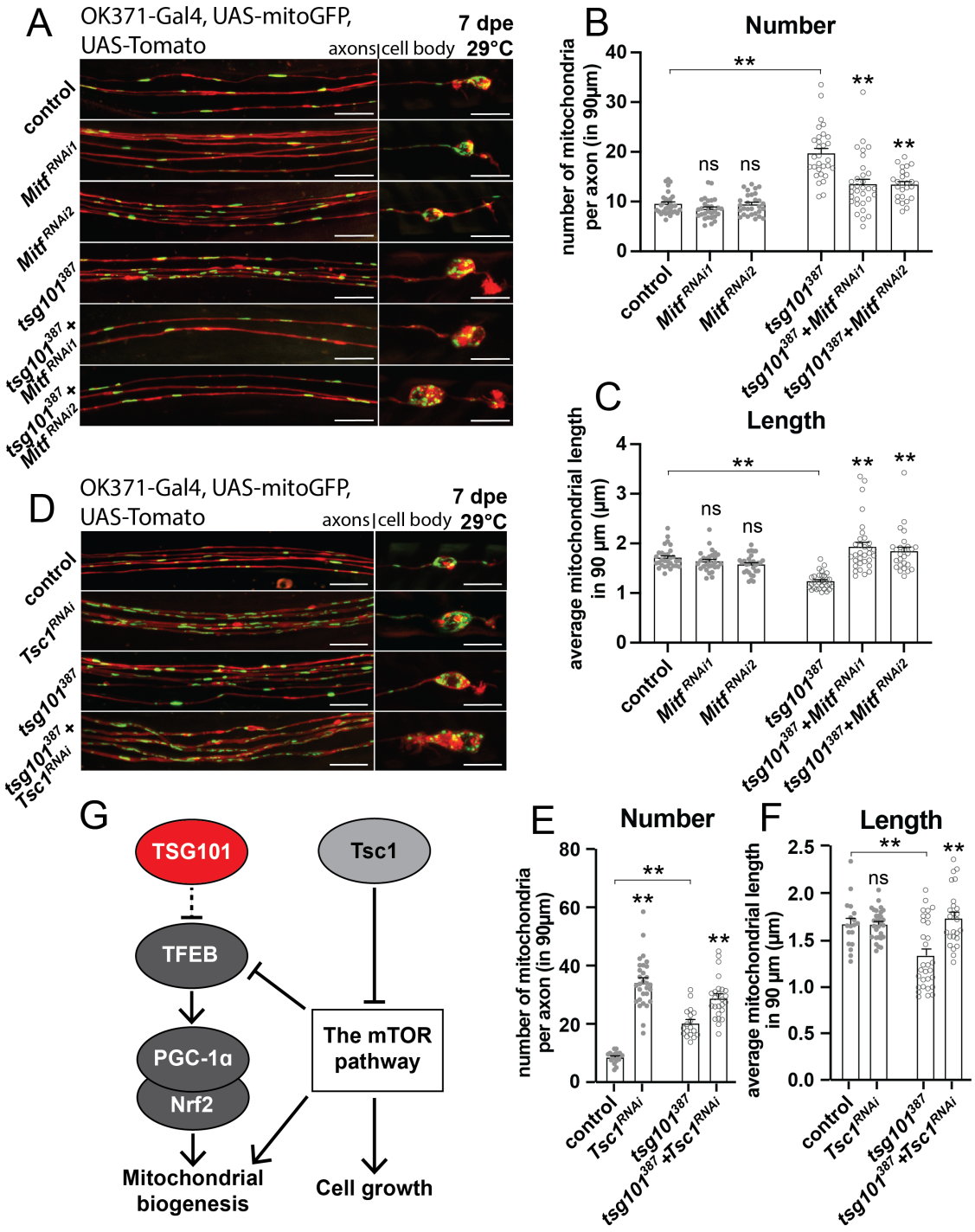

Fig. 5.3:

Homozygous mutant neurons were generated and labeled using the same approach as in the previous figure. **(A-C)** Two independent RNAis were used to knock down TFEB (*Mitf*), and both of them successfully suppressed the TSG101-mutant phenotype. The result is quantified in (B) and (C). **(D-F)** Tsc1 RNAi (BDSC:54034) was used to de-inhibit the mTOR pathway. Activating the mTOR pathway had no effect on the mitochondrial length in wildtype, and it even rescued TSG101mutants. However, mTOR activation led to a more than 3X increase in mitochondrial number in comparison to the control, and it even elevated the number in TSG101mutants, suggesting that the TSG101 and the mTOR pathways are parallel. Quantifications are shown in (E) and (F). All data were analyzed via two-way ANOVA, with at least 30 wings (one wing/animal) examined in each genotype ($N \geq 30$). Error bar: SEM. $^{**}p<0.01$. Scale bar: 10 μm. **(G)** A schematic model shows the novel genetic pathway of TSG101-controlled mitochondrial biogenesis and its relation with the mTOR pathway. In axons mutant for TSG101, TFEB-dependent mitochondrial biogenesis is activated, which requires PGC-1α and Nrf2. As studies have shown that the mTOR pathway suppresses TFEB activity and activates mitochondrial biogenesis through transcription factors other than Nrf2, TSG101-controlled mitochondrial biogenesis is parallel to the mTOR pathway.

Fig. 5.4: Whole-animal starvation did not lead to TSG101-mutant mitochondrial phenotype.

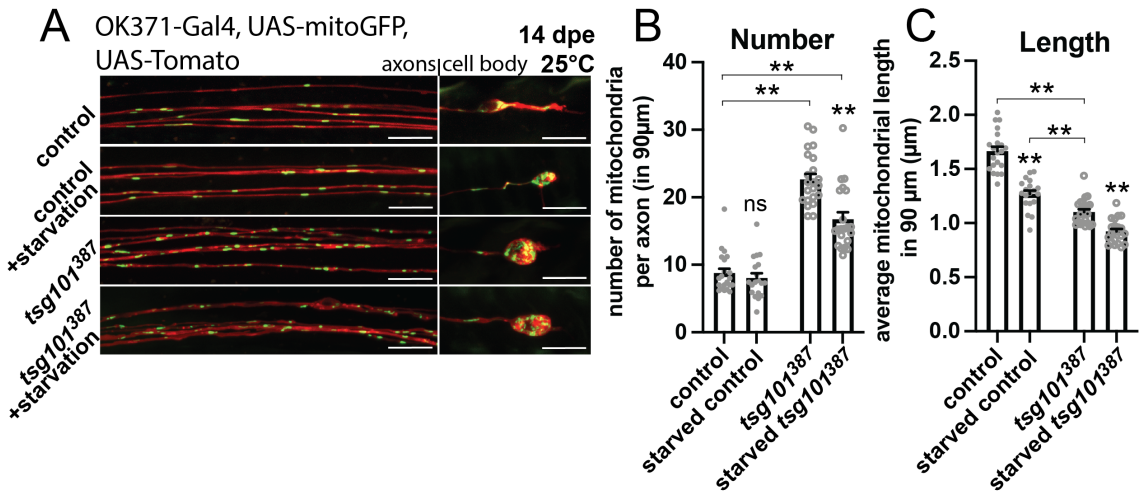

Fig. 5.4:

(A-C) Homozygous mutant neurons were generated and labeled as in the previous figure. Flies were raised in 25℃ and imaged at 14 dpe. Starved animals were grown in regular fly food media and then transferred to scarce media once eclosed (0-1 dpe). Quantifications of mitochondrial number and size are shown in (B) and (C) respectively. At least 20 wings (one wing/animal) were examined in each genotype (N≥20). All data were analyzed via two-way ANOVA. Error bar: SEM. $^{**}p<0.01$. Scale bar: 10 µm.

Fig. 5.5: Epistatic analysis of fission-fusion and TSG101.

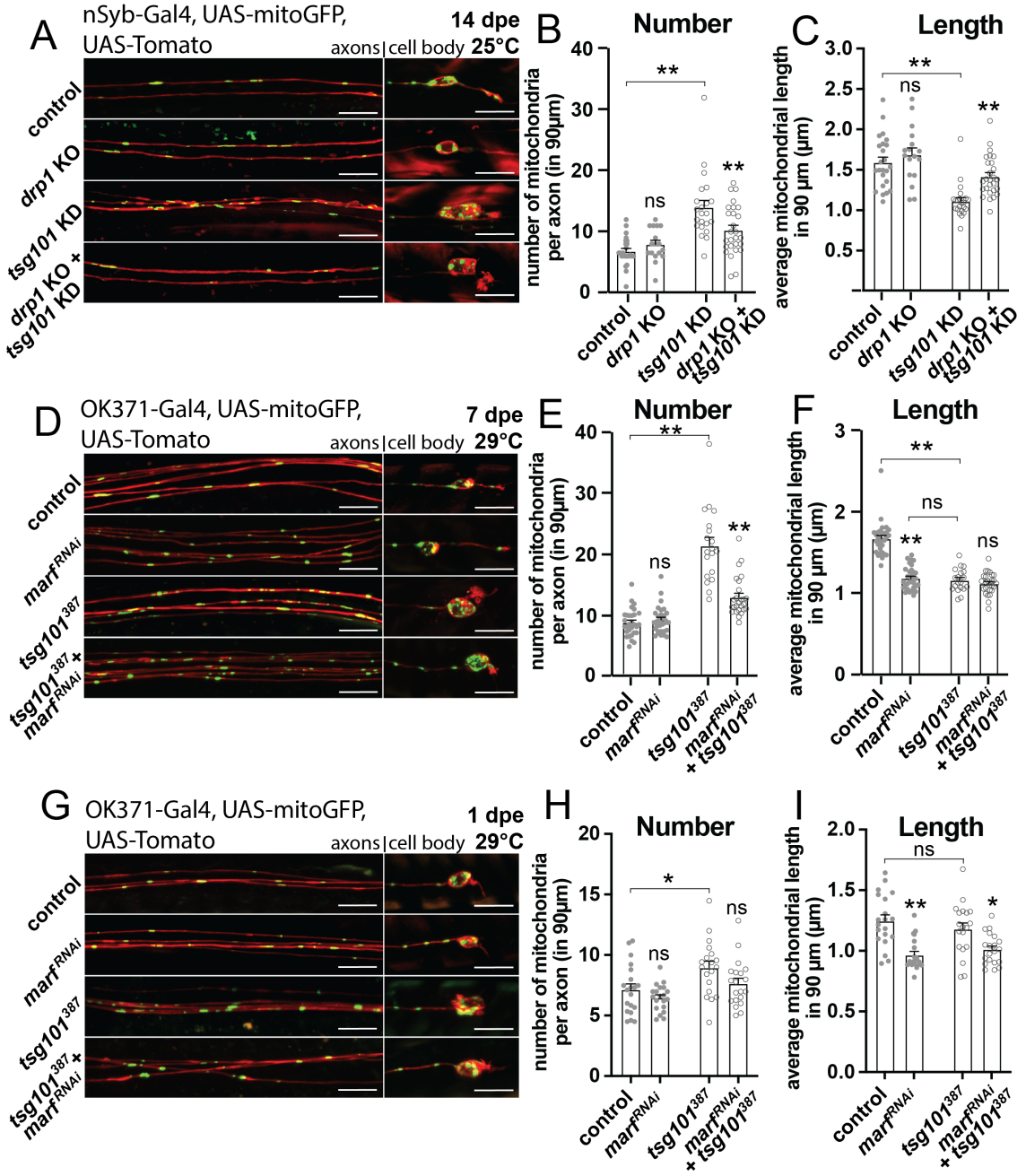

Fig. 5.5:

Mutant neurons were generated and labeled as described in Chapter 2. **(A-C)** Drp1 was knocked out to suppress mitochondrial fission to suppress the TSG101-knockdown phenotype, which is similar to TSG101 knockout. Both mitochondrial number and length were rescued by Drp1 knockout, demonstrating that mitochondrial fission is the final step of biogenesis. Flies were grown in 25℃ and the neurons were examined at 14 dpe. Quantification of axonal mitochondria is shown in (B) and (C). **(D-I)** $marf^{RNAi}$ was used to inhibit mitochondrial fusion in order to recapitulate the TSG101-mutant mitochondrial phenotype at 7 dpe (D-F) and 1dpe (G-I). To our surprise, Marf knockdown rescued the number at 7 dpe (E), suggesting Marf is involved in TSG101-dependent mitochondrial biogenesis. Flies were kept in 29℃ and the neurons were examined at 7 dpe and 1 dpe. Quantification of 7dpe is shown in (E) and (F), and 1dpe in (H) and (I). Data were analyzed via two-way ANOVA, with about 20 animals examined in each genotype ($N \cong 20$). *$p>0.05$. **$p<0.01$. Error bar: SEM. Scale bar: 10 μm.

Chapter 6: TSG101 regulates mitochondria and neurodegeneration through independent pathways

Results

TSG101 depletion leads to spontaneous neurodegeneration as animals age (Fig. 2.3A). How does the lack of TSG101 lead to neurodegeneration? Since mitochondria have been associated with neurodegeneration, I explored the relationship between neurodegeneration and mitochondrial phenotype. Given that knockdown of TFEB or Nrf2 restored both mitochondrial numbers and sizes in TSG101 mutants (Fig. 5.2, 5.3), we explored whether these manipulations also prevented neurodegeneration. However, knocking down TFEB (Mitf) and Nrf2 (Cnc) had no effect on either neurodegeneration or axon survival rate, even though TSG101-muatant mitochondrial phenotypes were completely suppressed (Fig. 6.1A, B). This finding supports the hypothesis that TSG101 has two roles, one to inhibit biogenesis and another to maintain long-term neuronal integrity.

To further investigate how loss of TSG101 contributes to neuronal death, I used a variety of well-established genetic inhibitors of axon degeneration and cell death—Wld^{s}, $p53^{DN}$, and p35—to block Wallerian degeneration and apoptotic pathways (Avery et al., 2012; Hay et al., 1994; Ollmann et al., 2000). Interestingly, neither suppression of Wallerian degeneration signaling nor blockade of apoptotic pathways stopped neurodegeneration (Fig. 6.1C), indicating that the neurodegeneration caused by lack of TSG101 occurs through a distinct mechanism. How the loss of TSG101 triggers neurodegeneration remains an interesting question. Since TSG101 has been associated

with spongiform neurodegeneration (He, 2003; Jiao et al., 2009; Kim et al., 2007), future studies on neurodegeneration that are independent of mitochondria as well as the Wallerian and apoptotic signaling pathways would greatly advance the understanding of the field.

Material & Methods

Drosophila *strains*

The following RNAi lines and over-expression constructs were used in an attempt to rescue TSG101-dependent neurodegeneration: *UAS-Wld^{S}* (lab stock, (Avery et al., 2009)), *UAS-p53.H159N* (dominant negative, BDSC:8420), *UAS-p35* (BDSC:5072), *5xUAS-cnc^{RNAi}* (BDSC:40854), and *5xUAS-Mitf^{RNAi}* (BDSC:44561). The following flies were used for MARCM clone generation: *OK371-Gal4* (BDSC:26160), *10xUAS-IVS-myr::td-Tomato* (BDSC:32222), *5xUAS-mito::EGFP* (BDSC:8442), *asense-FLP2e* (lab stock); *tub-Gal80* (BDSC:5190), *FRT2A* (BDSC:1997), and *FRT82B* (BDSC:2035).

Microscopy and image analysis

Images were acquired from a Zeiss spinning disc confocal microscope along with its proprietary Zen Blue software. Image processing was done with Zen Blue. All statistical analyses were conducted by using Graph Pad Prism 8. Data were analyzed via two-way ANOVA, with at least 15 wings (one wing/animal) examined in each genotype ($N \geq 15$).

Figures

Fig. 6.1: TSG101 knockout led to neurodegeneration in the late stage of adulthood via a distinct pathway independent of mitochondria, apoptosis, and Wallerian degeneration.

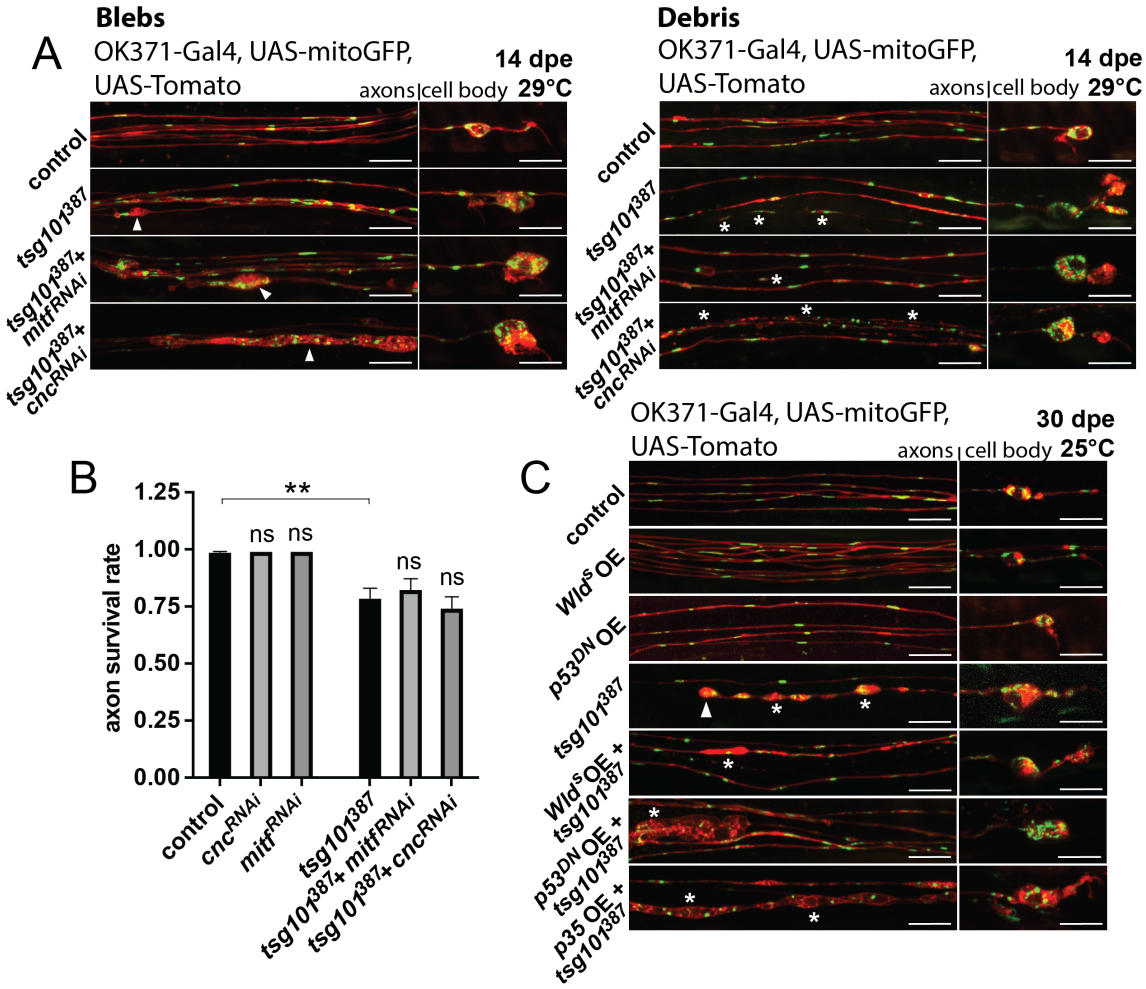

Fig. 6.1:

Homozygous mutant neurons were generated and labeled as in the previous figure. **(A)** *Mitf*^{RNAi1} and *cnc*^{RNAi1} used in Fig. 5.2 and 5.3 were able to suppress TSG101-mutant mitochondrial phenotype, and therefore were applied here to test whether neurodegeneration could also be prevented. Loss of axon maintenance could be seen in the forms of blebs (left panel, arrowheads) and debris (right panel, asterisks) in TSG101 mutants at 14 dpe 29℃. Knockdown of Mitf and Cnc in TSG101-mutant clones still exhibited neurodegeneration, with no change in axon survival rate (B). **(B)** Given that the cell bodies of the neurons remained visible long after the axons degenerated, the axon survival rates were calculated by the number of intact axons divided by the total number of the cell bodies. Data were analyzed via two-way ANOVA. N≥15. $^{**}p<0.01$. **(C)** Over-expression of *Wld*^{s} was used to stop Wallerian axon degeneration. Over-expressing *p53*^{DN} or *p35* was used to block apoptosis. Neurodegeneration could still be detected in TSG101 mutants (asterisks: blebs; arrowhead: axon stump) at 30 dpe 25℃, even though Wallerian degeneration or apoptosis was blocked. Scale bar: 10 μm.

Chapter 7: Discussion

All cell types dedicate a great number of resources to maintain an adequate number of functional mitochondria for a myriad of biological processes—and for neurons, the remarkable size and morphological complexity of axons, which can be thousands of times the volume of the cell body, present an enormous challenge. How does the neuron establish and maintain a healthy population of mitochondria at sufficient density throughout their axonal arbors? Healthy mitochondrial populations in axons are believed to be maintained primarily by mitochondrial transport into the axon (*i.e.* motility), anchoring, and fission-fusion to fine-tune mitochondrial functions accordingly. Turnover of damaged mitochondria or their components is mediated by mitochondrial AAA+ proteases, MDVs, mitophagy, or the general cellular degradative macro-autophagy pathway. Mitochondrial biogenesis is carried out by the activation of master transcription co-activator PGC-1α and its binding partner transcription factors, which leads to mitochondrial gene expression from the nucleus.

Neuronal mitochondrial homeostasis is constantly played out successfully throughout the animal's lifespan in order to sustain energetically demanding processes such as neurotransmission and to maintain neuronal integrity. The importance of neuronal mitochondrial homeostasis is borne out by the fact that mutations in many genes that regulate mitochondria lead to devastating neurological disorders and neurodegeneration. Despite our extensive knowledge of mitochondrial regulation, the full picture of mitochondrial homeostasis in axons remains incomplete. To begin to fill the gaps in our understanding, a former postdoctoral fellow Dr. Gaynor Smith and I designed and performed a forward genetic screen, which is unbiased and high-throughput, for mutants

that show altered mitochondrial dynamics, morphology, or both, in sensory axons in the *Drosophila* adult L1 wing vein *in vivo*. Gaynor identified Gzfz, a glutathione S-transferase that maintained GSH:GSSG balance; loss of Gfzf led to increased levels of GSSG, activation of Marf, and the subsequent mitochondrial fusion. I myself isolated four mutants—*2L.316*, *2L.409*, *3R.1054* and *3L.387*—and among these, *3L.387* was the most interesting. I discovered that *3L.387* exhibited increased mitochondrial number and decreased mitochondrial size in axons, and spontaneous neurodegeration at the late stages of adulthood. Further characterization showed that *3L.387* is a new null allele of TSG101, a well-known component of the ESCRT-I complex. TSG101 has been associated with neurodegeneration in the literature, but had yet to be identified as required for maintaining mitochondrial numbers and sizes. Although I found that Shrb, a component of the ESCRT-III complex, was also required for axonal mitochondrial homeostasis, like TSG101, I found no evidence that the other components of the ESCRT machinery were involved in regulating mitochondria in axons. This supports the notion that TSG101 and Shrb regulate mitochondrial numbers and sizes in a non-canonical pathway. After a series of investigation using genetic approaches, I discovered that the mutant mitochondrial phenotype was perhaps not caused by the lack of mitochondrial turnover, but by mitochondrial fission mediated by mitochondria biogenesis that is TFEB-, PGC-1α-, and Nfr2-dependent. Moreover, although knockdown of TFEB or Nfr2 successfully restored mitochondrial numbers and sizes in TSG101-mutant background, the TSG101-dependent neurodegeneration was not suppressed with the same approach, indicating a dissociation between mitochondria and TSG101-dependent neurodegeneration (Fig. 7.1).

Two other components of the ESCRT complexes have recently been linked to mitophagy or autophagy in cultured cells. CHMP2A/Vps2 of ESCRT-III was found to promote mitophagy by mediating phagophore sealing during autophagy; Snf8/Lsn of ESCRT-II was discovered to be important in autophagy-independent but endosome-dependent mitochondrial clearance (Hammerling et al., 2017). However, knockout of either of these genes (Chapter 3), or full blockade of Parkin/PINK1 mitophagy or autophagy (Chapter 4), failed to recapitulate the TSG101-mutant phenotype. Although mitophagy is critical for mitochondrial turnover in many settings, these mechanisms have been studied primarily in the context of cellular stress (*e.g.* perturbation of mitochondrial membrane potential), while I examined the turnover in wild-type axons *in vivo*, which may account for some differences in the genetic pathways deployed. Indeed, others have also found that loss of PINK1 or Parkin do not alter axonal mitochondria significantly *in vivo* (Lee et al., 2018; McWilliams et al., 2018). I therefore interpret my data to indicate that at least one component of the ESCRT complex, TSG101, may function in mitophagy regulation under chronic stress and yet under normal physiological conditions functions instead as a negative regulator of mitochondrial biogenesis.

Given the fact that I observed mitochondrial turnover events in axons by using mito-QC (Chapter 4), turnover of mitochondria appears to happen in the axons of *Drosophila* sensory neurons. These may be mediated by MDVs, which are normally shed in control animals and turned over through lysosomal-dependent mechanisms to maintain a functional mitochondria pool in axons. The mechanisms by which turnover occurs in axons is unclear, but they are likely independent of PINK1, Parkin and autophagy, since their full blockade did not alter mitochondrial numbers in axons. My data indicate that

there is likely another lysosome-mediated pathway that selectively targets MDVs for turnover. Whatever the pathway is, it appears sensitive to loss of TSG101: in TSG101 mutants, we found a near complete blockade of turnover of mitochondrial components based on the mito-QC results.

Live cell imaging revealed an accumulation of endolysosomes in the axon, which may occur through a compounded effect of the absence of autophagosome-lysosome fusion and activated lysosomal biogenesis due to the disinhibition of TFEB. Loss of TSG101 caused an increased proportion of stationary lysosomes in close proximity to mitochondria without subsequent sequestration, and since mitochondrial turnover was attenuated, this finding indicates a deficit in trafficking of mitochondria, or possibly MDVs in axons, to lysosomes. It is also possible that the stationary late endosomes/lysosomes in close proximity may facilitate mitochondrial biogenesis by serving as translation hubs for mitochondrial encoded proteins, a phenomenon that has been previously reported (Cioni et al., 2019).

How TSG101 regulates mitochondrial numbers in axons through regulation of biogenesis is an interesting question. Loss of TSG101 resulted in increased numbers of smaller mitochondria, and the measurements of mitochondrial physiology indicate that these mitochondria had fewer oxidative species and heightened OXPHOS than in controls (Chapter 5). These features suggest that TSG101 mutant axons shift towards increased mitochondrial biogenesis, and therefore I argue that TSG101 normally functions constitutively to suppress mitochondrial biogenesis. It would be interesting to see in future studies if loss of TSG101 also enhances mitochondrial membrane potential. How does TSG101 control mitochondrial biogenesis? One model is that TSG101 somehow conveys

signaling back to the nucleus to inhibit activation of the nuclear transcriptional program mediated by PGC-1α, Nrf2, and TFEB, which are key regulators of nuclear mitochondrial genes. In addition, previous work has shown that TFEB is held on lysosomes when it is not active, and it is released and translocates to the nucleus for transcription upon deactivation of the mTOR pathway (Settembre et al., 2012). It is therefore possible that TSG101 might control TFEB in a similar fashion.

Changes in mitochondria occur in *Drosophila* axons with aging. In wild-type animals, mitochondrial numbers remain fairly constant, but average mitochondrial length increases with age. Interestingly, however, mitochondrial number in TSG101 mutants increased over time, while mitochondrial length remained short even at late time points, in contrast to wild-type where an age-dependent increase was observed. As shown before, mitochondrial number and size in TSG101 knockdown conditions can be rescued by knockout of Drp1 (Chapter 5), a result that is consistent with the notion that the final step of mitochondrial biogenesis requires fission (Amiri and Hollenbeck, 2008). I also found that, strangely, elevated mitochondrial numbers in TSG101-null clones were rescued by knockdown of Marf, which should enhance fusion. That manipulating fusion can rescue mutant phenotypes seems counter-intuitive and requires further explanation. PGC-1α can activate Mfn2 (a Marf homolog) in mammalian cells (Cartoni et al., 2005; Van Laar et al., 2018); to expand to a sizable number of mitochondria (i.e. mitochondrial biogenesis), Marf and/or mitochondrial fusion are required in order to grow mitochondria in size before fission initiates, severing and generating mitochondria from the existing ones. Certainly, overexpression of PCG-1α has also been found to increase the phosphorylation of Drp1 to enhance fusion (Peng et al., 2017). In the TSG101-knockout and Marf-knockdown

condition, mitochondrial fusion was blocked and fission was no longer required, hence the inhibition of TSG101-dependent growth in mitochondrial number. How high levels of fission and fusion coordinate with one another to expand a mitochondrial pool in a developing neuron is an interesting and important question for future studies. There is also a possibility that manipulating fusion/fission dynamics can feed back and change how PGC-1α signals downstream of TSG101. Understanding how this feedback mechanism might work is potentially important and requires further investigation.

I found that the loss of TSG101 causes age-dependent neurodegeneration that occurs independently of changes in mitochondrial dynamics. Prior to cell death, axons are swollen and dysmorphic, recapitulating spongiform phenotypes observed in MGRN1-knockout mice (He, 2003; Jiao et al., 2009; Kim et al., 2007), which is associated with loss of TSG101. Genetic blockade of either apoptosis or Wallerian degeneration did not prevent such neurodegeneration, indicating a unique form of cell death. Spongiform-like degeneration could be the direct consequence of the accumulation of endolysosomes or the loss of the receptor cargos they contain.

Can mitochondrial biogenesis happen in the axons? BrdU labeling studies in isolated chick neurons support the notion that at least *in vitro* mitochondrial biogenesis can occur in axons (Amiri and Hollenbeck, 2008) and could be triggered by oxidative stress (Van Laar et al., 2018), and it seems likely that biogenesis happens in axons *in vivo*, especially in very long axons that cannot as easily derive such support from the soma. Mitochondrial numbers or position may also meaningfully regulate neurophysiology. Intriguingly, loss of Syntaphilin, a molecule that anchors mitochondria to the cytoskeleton, leads to widespread mitochondrial motility in neurites. Enhanced mitochondrial motility

correlated with increased pulse-to-pulse variability in synaptic properties, while anchoring mitochondria reduced variability (Sun et al., 2013). The primary effect of mitochondria appeared to be through changes in ATP levels (Sun et al., 2013), which we also observed in TSG101-mutant axons. An exciting next question is whether axon-specific regulation of mitochondrial biogenesis or clearance can also provide an additional mechanism to contribute to cell-specific plasticity in circuits.

Altogether, although the discovery of the novel mitochondrial modulators we have identified so far do not fully address the main question of the field—how is the large pool of axonal mitochondria maintained in the long stretches of axons *in vivo*—it certainly put our foot in the door. How are mitochondrial numbers, sizes, and localities determined in axons *in vivo*? As we did not unravel any new regulators of mitochondrial transport in the screen, we did not gain any new insight of mitochondrial mobility and locality. However, we did find that the main forces governing mitochondrial numbers and sizes in axons are also mitochondrial fission and fusion, and we started to discover a variety of new upstream mechanisms that regulate them: fusion can be controlled by glutathione S-transferases (*e.g.* Gfzf) which regulate the GSH:GSSG balance, and fission mediated by mitochondrial biogenesis is constantly inhibited by an ESCRT component TSG101 (Fig. 7.1A). Both Gfzf and TSG101 may endow the neuron the ability to maintain mitochondrial dynamics locally in the axon compartment, but cell-wide changes such as mitochondrial biogenesis certainly rely on the support of the cell body. Although the detailed mechanism by which TSG101 regulates TFEB and hence mitochondrial biogenesis needs further investigation, our data so far suggests that TSG101 might be one of the molecules that allow the neuron to regulate mitochondrial production according to its size and needs. How are mitochondria turned

over in axons? Parkin/PINK1-mediated mitophagy and macroautophagy are the main pathways that turn mitochondria over in the cell body, however the axons utilize an independent mechanism. Although we do not fully understand how axonal mitochondria are cleared, we certainly know it depends on TSG101. I believe that saturating the forward genetic screen may help us discover more novel mitochondrial modulators so that we may get the full picture of how mitochondrial homeostasis is maintained in axons *in vivo*. As I provided evidence showing that TSG101-dependent neurodegeneration is independent of Wallerian degeneration, apoptosis, and, most importantly, mitochondria, I also believe that the screen might also give us a clearer understanding of different types of neurodegenerations and the mechanisms behind them.

Figures

Fig. 7.1: A schematic summary—the isolated mutants from the forward genetic screen and their phenotypes.

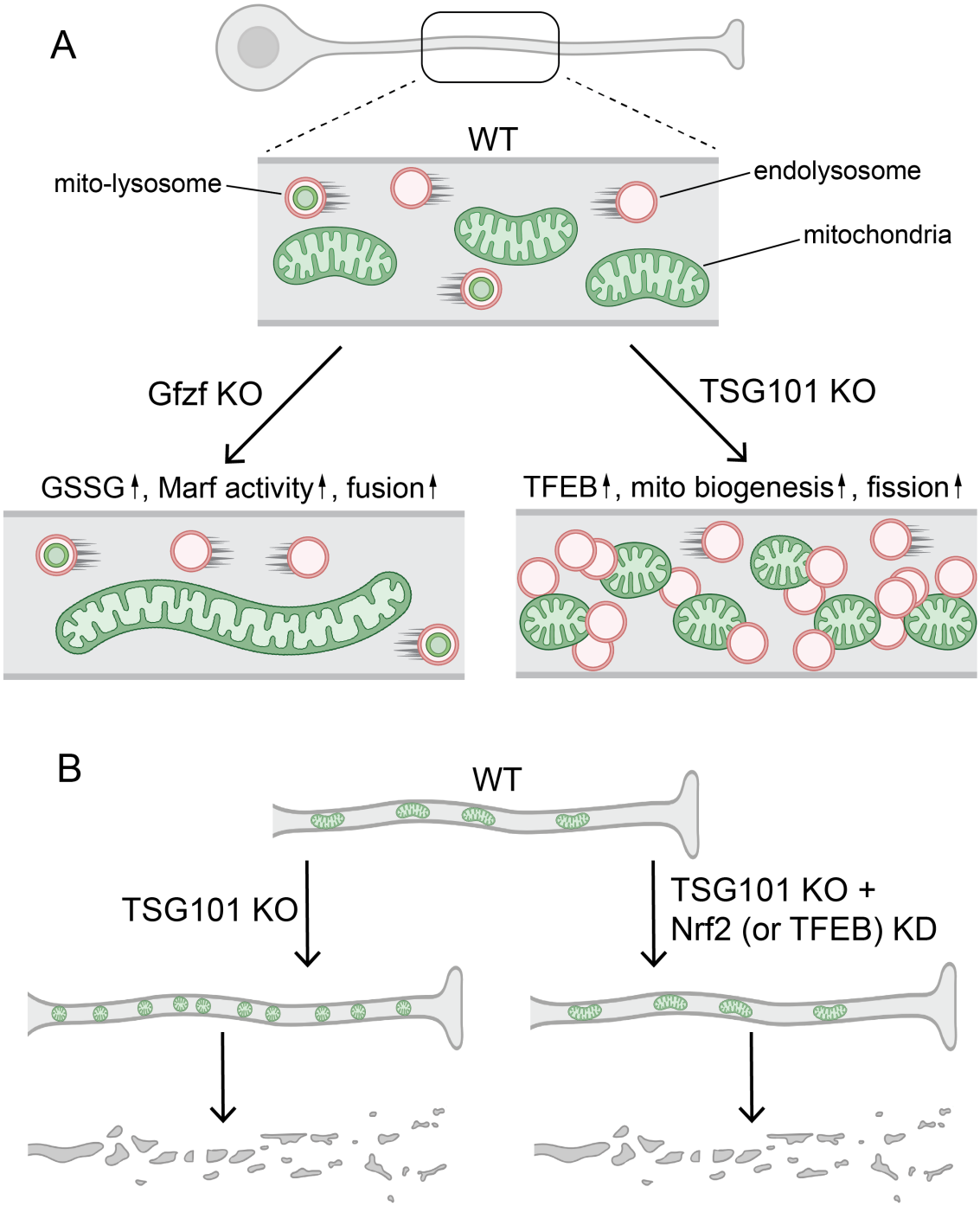

Fig 7.1:

(A) A schematic summary of how mitochondrial dynamics are changed upon Gfzf or TSG101 ablation. Loss of Gfzf leads to mitochondrial fusion—following Gfzf knockout (Gfzg KO), GSH is increased drastically and rapidly converted into GSSG, leading to GSSG accumulation, which in turn triggers Marf oligomerization and mitochondrial fusion. Loss of TSG101, however, results in mitochondrial fission. TSG101-mutant axons exhibited increased mitochondrial number, decreased mitochondrial size, disrupted endolysosomal trafficking, lack of mitochondrial turnover (or, specifically, lack of mito-lysosomes), and spontaneous neurodegeneration. Upon TSG101 ablation, TFEB, a master transcription factor of lysosomal biogenesis, is activated, and that in turn triggers mitochondrial biogenesis and the subsequent mitochondrial fission by activating PGC-1α and Nrf2. In addition, the dramatic accumulation of endolysosomes might be the compounded effect of activated lysosomal biogenesis by TFEB and lack of mitochondrial trafficking to the endolysosomes. **(B)** Loss of TSG101 leads to axon degeneration, which cannot be suppressed by rescuing mitochondria via knockdown of Nrf2 or TFEB, suggesting that TSG101-dependent axon degeneration is independent of mitochondria. This figure was created with BioRender.com.

Summary & Conclusions

Mitochondrial dysfunction has been associated with many age-dependent neurodegenerative disorders such as Parkinson's and Alzheimer's disease, yet understanding how a neuron maintains a pool of functional mitochondria in sufficient density and location throughout large stretches of axon *in vivo* remains understudied. To unravel new genes or novel mechanisms that are important for axonal mitochondrial biology, a former post-doctoral fellow Dr. Gaynor Smith and I designed and performed an unbiased *in vivo* forward genetic screen, through which Gaynor identified Gfzf, a glutathione S-transferase that keeps mitochondrial fusion in check by maintaining GSH:GSSG homeostasis. Meanwhile, I identified three candidates and TSG101, an ESCRT component, as a new regulator of mitochondrial number and size in neurons. I not only provide evidence to demonstrate the role of TSG101 as a negative regulator of mitochondrial biogenesis, but also find that TSG101 does not play a role in Parkin/PINK1-mediated mitophagy and that macroautophagy is dispensable in axonal mitochondrial regulation *in vivo*. Lastly, TSG101 has been associated with spongiform neurodegeneration, and I show evidence that such neurodegeneration occurs via a yet unknown mechanism. Taken together, my findings suggest that, through unbiased *in vivo* neuronal screening, it is possible to unravel translatable mechanisms important for mitochondrial homeostasis and axonal maintenance, and to greatly advance our understanding of the mechanisms that drive neurodegeneration.

References

1. Albrecht, S.C., Barata, A.G., Großhans, J., Teleman, A.A., and Dick, T.P. (2011). In Vivo Mapping of Hydrogen Peroxide and Oxidized Glutathione Reveals Chemical and Regional Specificity of Redox Homeostasis. Cell Metab. *14*, 819–829.

2. Amiri, M., and Hollenbeck, P.J. (2008). Mitochondrial biogenesis in the axons of vertebrate peripheral neurons. Dev. Neurobiol. *68*, 1348–1361.

3. Ashrafi, G., Schlehe, J.S., LaVoie, M.J., and Schwarz, T.L. (2014). Mitophagy of damaged mitochondria occurs locally in distal neuronal axons and requires PINK1 and Parkin. J. Cell Biol. *206*, 655–670.

4. Avery, M.A., Sheehan, A.E., Kerr, K.S., Wang, J., and Freeman, M.R. (2009). WldS requires Nmnat1 enzymatic activity and N16–VCP interactions to suppress Wallerian degeneration. J. Cell Biol. *184*, 501–513.

5. Avery, M.A., Rooney, T.M., Pandya, J.D., Wishart, T.M., Gillingwater, T.H., Geddes, J.W., Sullivan, P.G., and Freeman, M.R. (2012). WldS prevents axon degeneration through increased mitochondrial flux and enhanced mitochondrial Ca2+ buffering. Curr. Biol. CB *22*, 596–600.

6. Babst, M., Odorizzi, G., Estepa, E.J., and Emr, S.D. (2000). Mammalian Tumor Susceptibility Gene 101 (TSG101) and the Yeast Homologue, Vps23p, Both Function in Late Endosomal Trafficking: TSG101 Functions in Late Endosomal Trafficking. Traffic *1*, 248–258.

7. Baloh, R.H., Schmidt, R.E., Pestronk, A., and Milbrandt, J. (2007). Altered Axonal Mitochondrial Transport in the Pathogenesis of Charcot-Marie-Tooth Disease from Mitofusin 2 Mutations. J. Neurosci. *27*, 422–430.

8. Berry, D.L., and Baehrecke, E.H. (2007). Growth Arrest and Autophagy Are Required for Salivary Gland Cell Degradation in Drosophila. Cell *131*, 1137–1148.

9. Brandt, T., Cavellini, L., Kühlbrandt, W., and Cohen, M.M. (2016). A mitofusin-dependent docking ring complex triggers mitochondrial fusion in vitro. ELife *5*, e14618.

10. Cai, Q., Zakaria, H.M., Simone, A., and Sheng, Z.-H. (2012). Spatial Parkin Translocation and Degradation of Damaged Mitochondria via Mitophagy in Live Cortical Neurons. Curr. Biol. *22*, 545–552.

11. Cartoni, R., Léger, B., Hock, M.B., Praz, M., Crettenand, A., Pich, S., Ziltener, J.-L., Luthi, F., Dériaz, O., Zorzano, A., et al. (2005). Mitofusins 1/2 and ERRα expression are increased in human skeletal muscle after physical exercise: Mitofusins 1/2 and ERRα expression in skeletal muscle. J. Physiol. *567*, 349–358.

12. Chang, D.T.W., and Reynolds, I.J. (2006). Differences in mitochondrial movement and morphology in young and mature primary cortical neurons in culture. Neuroscience *141*, 727–736.

13. Chen, Y., and Dorn, G.W. (2013). PINK1-Phosphorylated Mitofusin 2 Is a Parkin Receptor for Culling Damaged Mitochondria. Science *340*, 471–475.

14. Chen, C., Liu, Y., Liu, R., Ikenoue, T., Guan, K.-L., Liu, Y., and Zheng, P. (2008). TSC–mTOR maintains quiescence and function of hematopoietic stem cells by repressing mitochondrial biogenesis and reactive oxygen species. J. Exp. Med. *205*, 2397–2408.

15. Cho, D.-H., Nakamura, T., and Lipton, S.A. (2010). Mitochondrial dynamics in cell death and neurodegeneration. Cell. Mol. Life Sci. CMLS *67*, 3435–3447.

16. Cioni, J.-M., Lin, J.Q., Holtermann, A.V., Koppers, M., Jakobs, M.A.H., Azizi, A., Turner-Bridger, B., Shigeoka, T., Franze, K., Harris, W.A., et al. (2019). Late Endosomes Act as mRNA Translation Platforms and Sustain Mitochondria in Axons. Cell *176*, 56-72.e15.

17. Cunningham, J.T., Rodgers, J.T., Arlow, D.H., Vazquez, F., Mootha, V.K., and Puigserver, P. (2007). mTOR controls mitochondrial oxidative function through a YY1–PGC-1α transcriptional complex. Nature *450*, 736–740.

18. Dominy, J.E., and Puigserver, P. (2013). Mitochondrial Biogenesis through Activation of Nuclear Signaling Proteins. Cold Spring Harb. Perspect. Biol. *5*, a015008–a015008.

19. Drerup, C.M., Herbert, A.L., Monk, K.R., and Nechiporuk, A.V. (2017). Regulation of mitochondria-dynactin interaction and mitochondrial retrograde transport in axons. ELife *6*, e22234.

20. Elgass, K.D., Smith, E.A., LeGros, M.A., Larabell, C.A., and Ryan, M.T. (2015). Analysis of ER–mitochondria contacts using correlative fluorescence microscopy and soft X-ray tomography of mammalian cells. J. Cell Sci. *128*, 2795–2804.

21. Evans, C.S., and Holzbaur, E.L.F. (2020). Quality Control in Neurons: Mitophagy and Other Selective Autophagy Mechanisms. J. Mol. Biol. *432*, 240–260.

22. Frank, M., Duvezin-Caubet, S., Koob, S., Occhipinti, A., Jagasia, R., Petcherski, A., Ruonala, M.O., Priault, M., Salin, B., and Reichert, A.S. (2012). Mitophagy is triggered by mild oxidative stress in a mitochondrial fission dependent manner. Biochim. Biophys. Acta *1823*, 2297–2310.

23. Fridell, Y.-W.C., Sánchez-Blanco, A., Silvia, B.A., and Helfand, S.L. (2005). Targeted expression of the human uncoupling protein 2 (hUCP2) to adult neurons extends life span in the fly. Cell Metab. *1*, 145–152.

24. Friedman, J.R., Lackner, L.L., West, M., DiBenedetto, J.R., Nunnari, J., and Voeltz, G.K. (2011). ER Tubules Mark Sites of Mitochondrial Division. Science *334*, 358–362.

25. Fukumitsu, K., Hatsukano, T., Yoshimura, A., Heuser, J., Fujishima, K., and Kengaku, M. (2016). Mitochondrial fission protein Drp1 regulates mitochondrial transport and dendritic arborization in cerebellar Purkinje cells. Mol. Cell. Neurosci. *71*, 56–65.

26. Gaston, D., Tsaousis, A.D., and Roger, A.J. (2009). Chapter 2 Predicting Proteomes of Mitochondria and Related Organelles from Genomic and Expressed Sequence Tag Data. In Methods in Enzymology, (Elsevier), pp. 21–47.

27. Giovarelli, M., Zecchini, S., Martini, E., Garrè, M., Barozzi, S., Ripolone, M., Napoli, L., Coazzoli, M., Vantaggiato, C., Roux-Biejat, P., et al. (2020). Drp1 overexpression induces desmin disassembling and drives kinesin-1 activation promoting mitochondrial trafficking in skeletal muscle. Cell Death Differ. *27*, 2383–2401.

28. Glynn, S.E. (2017). Multifunctional Mitochondrial AAA Proteases. Front. Mol. Biosci. *4*, 34.

29. Hammerling, B.C., Najor, R.H., Cortez, M.Q., Shires, S.E., Leon, L.J., Gonzalez, E.R., Boassa, D., Phan, S., Thor, A., Jimenez, R.E., et al. (2017). A Rab5 endosomal pathway mediates Parkin-dependent mitochondrial clearance. Nat. Commun. *8*, 14050.

30. Hay, B.A., Wolff, T., and Rubin, G.M. (1994). Expression of baculovirus P35 prevents cell death in Drosophila. Development *120*, 2121.

31. He, L. (2003). Spongiform Degeneration in mahoganoid Mutant Mice. Science *299*, 710–712.

32. Hewitt, V.L., and Whitworth, A.J. (2017). Mechanisms of Parkinson's Disease. In Current Topics in Developmental Biology, (Elsevier), pp. 173–200.

33. Jiao, J., Sun, K., Walker, W.P., Bagher, P., Cota, C.D., and Gunn, T.M. (2009). Abnormal regulation of TSG101 in mice with spongiform neurodegeneration. Biochim. Biophys. Acta BBA - Mol. Basis Dis. *1792*, 1027–1035.

34. Jodeiri Farshbaf, M., and Ghaedi, K. (2017). Huntington's Disease and Mitochondria. Neurotox. Res. *32*, 518–529.

35. Kim, B.Y., Olzmann, J.A., Barsh, G.S., Chin, L.-S., and Li, L. (2007). Spongiform Neurodegeneration-associated E3 Ligase Mahogunin Ubiquitylates TSG101 and Regulates Endosomal Trafficking. Mol. Biol. Cell *18*, 1129–1142.

36. Kitada, T., Asakawa, S., Hattori, N., Matsumine, H., Yamamura, Y., Minoshima, S., Yokochi, M., Mizuno, Y., and Shimizu, N. (1998). Mutations in the parkin gene cause autosomal recessive juvenile parkinsonism. Nature *392*, 605–608.

37. Koshiba, T. (2004). Structural Basis of Mitochondrial Tethering by Mitofusin Complexes. Science *305*, 858–862.

38. Lee, H., and Yoon, Y. (2016). Mitochondrial fission and fusion. Biochem. Soc. Trans. *44*, 1725–1735.

39. Lee, T., and Luo, L. (1999). Mosaic Analysis with a Repressible Cell Marker for Studies of Gene Function in Neuronal Morphogenesis. Neuron *22*, 451–461.

40. Lee, J.J., Sanchez-Martinez, A., Zarate, A.M., Benincá, C., Mayor, U., Clague, M.J., and Whitworth, A.J. (2018). Basal mitophagy is widespread in *Drosophila* but minimally affected by loss of Pink1 or parkin. J. Cell Biol. jcb.201801044.

41. Liu, X., Weaver, D., Shirihai, O., and Hajnóczky, G. (2009). Mitochondrial 'kiss-and-run': interplay between mitochondrial motility and fusion–fission dynamics. EMBO J. *28*, 3074–3089.

42. Lobas, M.A., Tao, R., Nagai, J., Kronschläger, M.T., Borden, P.M., Marvin, J.S., Looger, L.L., and Khakh, B.S. (2019). A genetically encoded single-wavelength sensor for imaging cytosolic and cell surface ATP. Nat. Commun. *10*, 711.

43. Low, H.H., and Löwe, J. (2006). A bacterial dynamin-like protein. Nature *444*, 766–769.

44. Maday, S., and Holzbaur, E.L.F. (2014). Autophagosome Biogenesis in Primary Neurons Follows an Ordered and Spatially Regulated Pathway. Dev. Cell *30*, 71–85.

45. Magrané, J., Cortez, C., Gan, W.-B., and Manfredi, G. (2014). Abnormal mitochondrial transport and morphology are common pathological denominators in SOD1 and TDP43 ALS mouse models. Hum. Mol. Genet. *23*, 1413–1424.

46. Maltecca, F., De Stefani, D., Cassina, L., Consolato, F., Wasilewski, M., Scorrano, L., Rizzuto, R., and Casari, G. (2012). Respiratory dysfunction by AFG3L2 deficiency causes decreased mitochondrial calcium uptake via organellar network fragmentation. Hum. Mol. Genet. *21*, 3858–3870.

47. Mansueto, G., Armani, A., Viscomi, C., D'Orsi, L., De Cegli, R., Polishchuk, E.V., Lamperti, C., Di Meo, I., Romanello, V., Marchet, S., et al. (2017).

Transcription Factor EB Controls Metabolic Flexibility during Exercise. Cell Metab. *25*, 182–196.

48. Martina, J.A., Chen, Y., Gucek, M., and Puertollano, R. (2012). MTORC1 functions as a transcriptional regulator of autophagy by preventing nuclear transport of TFEB. Autophagy *8*, 903–914.

49. Matheoud, D., Sugiura, A., Bellemare-Pelletier, A., Laplante, A., Rondeau, C., Chemali, M., Fazel, A., Bergeron, J.J., Trudeau, L.-E., Burelle, Y., et al. (2016). Parkinson's Disease-Related Proteins PINK1 and Parkin Repress Mitochondrial Antigen Presentation. Cell *166*, 314–327.

50. McLelland, G.-L., Soubannier, V., Chen, C.X., McBride, H.M., and Fon, E.A. (2014). Parkin and PINK1 function in a vesicular trafficking pathway regulating mitochondrial quality control. EMBO J. n/a-n/a.

51. McWilliams, T.G., Prescott, A.R., Allen, G.F.G., Tamjar, J., Munson, M.J., Thomson, C., Muqit, M.M.K., and Ganley, I.G. (2016). *mito* -QC illuminates mitophagy and mitochondrial architecture in vivo. J. Cell Biol. *214*, 333–345.

52. McWilliams, T.G., Prescott, A.R., Montava-Garriga, L., Ball, G., Singh, F., Barini, E., Muqit, M.M.K., Brooks, S.P., and Ganley, I.G. (2018). Basal Mitophagy Occurs Independently of PINK1 in Mouse Tissues of High Metabolic Demand. Cell Metab. *27*, 439-449.e5.

53. Misgeld, T., and Schwarz, T.L. (2017). Mitostasis in Neurons: Maintaining Mitochondria in an Extended Cellular Architecture. Neuron *96*, 651–666.

54. Mishra, P., Carelli, V., Manfredi, G., and Chan, D.C. (2014). Proteolytic Cleavage of Opa1 Stimulates Mitochondrial Inner Membrane Fusion and Couples Fusion to Oxidative Phosphorylation. Cell Metab. *19*, 630–641.

55. Misko, A., Jiang, S., Wegorzewska, I., Milbrandt, J., and Baloh, R.H. (2010). Mitofusin 2 Is Necessary for Transport of Axonal Mitochondria and Interacts with the Miro/Milton Complex. J. Neurosci. *30*, 4232–4240.

56. Mootha, V.K., Bunkenborg, J., Olsen, J.V., Hjerrild, M., Wisniewski, J.R., Stahl, E., Bolouri, M.S., Ray, H.N., Sihag, S., Kamal, M., et al. (2003). Integrated Analysis of Protein Composition, Tissue Diversity, and Gene Regulation in Mouse Mitochondria. Cell *115*, 629–640.

57. Napolitano, G., Esposito, A., Choi, H., Matarese, M., Benedetti, V., Di Malta, C., Monfregola, J., Medina, D.L., Lippincott-Schwartz, J., and Ballabio, A. (2018). mTOR-dependent phosphorylation controls TFEB nuclear export. Nat. Commun. *9*, 3312.

58. Narendra, D., Tanaka, A., Suen, D.-F., and Youle, R.J. (2008). Parkin is recruited selectively to impaired mitochondria and promotes their autophagy. J. Cell Biol. *183*, 795–803.

59. Narendra, D.P., Jin, S.M., Tanaka, A., Suen, D.-F., Gautier, C.A., Shen, J., Cookson, M.R., and Youle, R.J. (2010). PINK1 Is Selectively Stabilized on Impaired Mitochondria to Activate Parkin. PLoS Biol. *8*, e1000298.

60. Neukomm, L.J., Burdett, T.C., Gonzalez, M.A., Züchner, S., and Freeman, M.R. (2014). Rapid in vivo forward genetic approach for identifying axon death genes in *Drosophila*. Proc. Natl. Acad. Sci. *111*, 9965–9970.

61. Neuspiel, M., Schauss, A.C., Braschi, E., Zunino, R., Rippstein, P., Rachubinski, R.A., Andrade-Navarro, M.A., and McBride, H.M. (2008). Cargo-Selected Transport from the Mitochondria to Peroxisomes Is Mediated by Vesicular Carriers. Curr. Biol. *18*, 102–108.

62. Nunnari, J., and Suomalainen, A. (2012). Mitochondria: in sickness and in health. Cell *148*, 1145–1159.

63. Ollmann, M., Young, L.M., Di Como, C.J., Karim, F., Belvin, M., Robertson, S., Whittaker, K., Demsky, M., Fisher, W.W., Buchman, A., et al. (2000). Drosophila p53 is a structural and functional homolog of the tumor suppressor p53. Cell *101*, 91–101.

64. Pagliarini, D.J., Calvo, S.E., Chang, B., Sheth, S.A., Vafai, S.B., Ong, S.-E., Walford, G.A., Sugiana, C., Boneh, A., Chen, W.K., et al. (2008). A Mitochondrial Protein Compendium Elucidates Complex I Disease Biology. Cell *134*, 112–123.

65. Park, J.-S., Davis, R.L., and Sue, C.M. (2018). Mitochondrial Dysfunction in Parkinson's Disease: New Mechanistic Insights and Therapeutic Perspectives. Curr. Neurol. Neurosci. Rep. *18*, 21.

66. Peng, K., Yang, L., Wang, J., Ye, F., Dan, G., Zhao, Y., Cai, Y., Cui, Z., Ao, L., Liu, J., et al. (2017). The Interaction of Mitochondrial Biogenesis and Fission/Fusion Mediated by PGC-1α Regulates Rotenone-Induced Dopaminergic Neurotoxicity. Mol. Neurobiol. *54*, 3783–3797.

67. Plucińska, G., and Misgeld, T. (2016). Imaging of neuronal mitochondria in situ. Curr. Opin. Neurobiol. *39*, 152–163.

68. Raiborg, C., and Stenmark, H. (2009). The ESCRT machinery in endosomal sorting of ubiquitylated membrane proteins. Nature *458*, 445–452.

69. Roberts, R.F., Tang, M.Y., Fon, E.A., and Durcan, T.M. (2016). Defending the mitochondria: The pathways of mitophagy and mitochondrial-derived vesicles. Int. J. Biochem. Cell Biol. *79*, 427–436.

70. Salvadores, N., Sanhueza, M., Manque, P., and Court, F.A. (2017). Axonal Degeneration during Aging and Its Functional Role in Neurodegenerative Disorders. Front. Neurosci. *11*, 451.

71. Saxton, W.M., and Hollenbeck, P.J. (2012). The axonal transport of mitochondria. J. Cell Sci. *125*, 2095–2104.

72. Schindelin, J., Arganda-Carreras, I., Frise, E., Kaynig, V., Longair, M., Pietzsch, T., Preibisch, S., Rueden, C., Saalfeld, S., Schmid, B., et al. (2012). Fiji: an open-source platform for biological-image analysis. Nat. Methods *9*, 676–682.

73. Schwarz, T.L. (2013). Mitochondrial Trafficking in Neurons. Cold Spring Harb. Perspect. Biol. *5*, a011304–a011304.

74. Settembre, C., Zoncu, R., Medina, D.L., Vetrini, F., Erdin, S., Erdin, S., Huynh, T., Ferron, M., Karsenty, G., Vellard, M.C., et al. (2012). A lysosome-to-nucleus signalling mechanism senses and regulates the lysosome via mTOR and TFEB: Self-regulation of the lysosome via mTOR and TFEB. EMBO J. *31*, 1095–1108.

75. Settembre, C., De Cegli, R., Mansueto, G., Saha, P.K., Vetrini, F., Visvikis, O., Huynh, T., Carissimo, A., Palmer, D., Jürgen Klisch, T., et al. (2013). TFEB controls cellular lipid metabolism through a starvation-induced autoregulatory loop. Nat. Cell Biol. *15*, 647–658.

76. Sheng, Z.-H. (2014). Mitochondrial trafficking and anchoring in neurons: New insight and implications. J. Cell Biol. *204*, 1087–1098.

77. Shlevkov, E., and Schwarz, T.L. (2014). For Parkin, it's not all or nothing. EMBO J. *33*, 277–279.

78. Sickmann, A., Reinders, J., Wagner, Y., Joppich, C., Zahedi, R., Meyer, H.E., Schonfisch, B., Perschil, I., Chacinska, A., Guiard, B., et al. (2003). The proteome of Saccharomyces cerevisiae mitochondria. Proc. Natl. Acad. Sci. *100*, 13207–13212.

79. Smith, D.H. (2009). Stretch growth of integrated axon tracts: Extremes and exploitations. Prog. Neurobiol. *89*, 231–239.

80. Smith, G.A., Lin, T.-H., Sheehan, A.E., Van der Goes van Naters, W., Neukomm, L.J., Graves, H.K., Bis-Brewer, D.M., Züchner, S., and Freeman, M.R. (2019). Glutathione S-Transferase Regulates Mitochondrial Populations in Axons through Increased Glutathione Oxidation. Neuron S0896627319303745.

81. Soubannier, V., McLelland, G.-L., Zunino, R., Braschi, E., Rippstein, P., Fon, E.A., and McBride, H.M. (2012). A Vesicular Transport Pathway Shuttles Cargo from Mitochondria to Lysosomes. Curr. Biol. *22*, 135–141.

82. Stavoe, A.K.H., and Holzbaur, E.L.F. (2019). Autophagy in Neurons. Annu. Rev. Cell Dev. Biol. *35*, 477–500.

83. Sun, T., Qiao, H., Pan, P.-Y., Chen, Y., and Sheng, Z.-H. (2013). Motile axonal mitochondria contribute to the variability of presynaptic strength. Cell Rep. *4*, 413–419.

84. Sung, H., Tandarich, L.C., Nguyen, K., and Hollenbeck, P.J. (2016). Compartmentalized Regulation of Parkin-Mediated Mitochondrial Quality Control in the Drosophila Nervous System In Vivo. J. Neurosci. *36*, 7375–7391.

85. Takahashi, Y., He, H., Tang, Z., Hattori, T., Liu, Y., Young, M.M., Serfass, J.M., Chen, L., Gebru, M., Chen, C., et al. (2018). An autophagy assay reveals the ESCRT-III component CHMP2A as a regulator of phagophore closure. Nat. Commun. *9*, 2855.

86. Twig, G., Liu, X., Liesa, M., Wikstrom, J.D., Molina, A.J.A., Las, G., Yaniv, G., Hajnóczky, G., and Shirihai, O.S. (2010). Biophysical properties of mitochondrial

fusion events in pancreatic β-cells and cardiac cells unravel potential control mechanisms of its selectivity. Am. J. Physiol.-Cell Physiol. *299*, C477–C487.

87. Vaccari, T., Rusten, T.E., Menut, L., Nezis, I.P., Brech, A., Stenmark, H., and Bilder, D. (2009). Comparative analysis of ESCRT-I, ESCRT-II and ESCRT-III function in Drosophila by efficient isolation of ESCRT mutants. J. Cell Sci. *122*, 2413–2423.

88. Valente, E.M. (2004). Hereditary Early-Onset Parkinson's Disease Caused by Mutations in PINK1. Science *304*, 1158–1160.

89. Van Laar, V.S., Arnold, B., Cassady, S.J., Chu, C.T., Burton, E.A., and Berman, S.B. (2011). Bioenergetics of neurons inhibit the translocation response of Parkin following rapid mitochondrial depolarization. Hum. Mol. Genet. *20*, 927–940.

90. Van Laar, V.S., Arnold, B., Howlett, E.H., Calderon, M.J., St. Croix, C.M., Greenamyre, J.T., Sanders, L.H., and Berman, S.B. (2018). Evidence for compartmentalized axonal mitochondrial biogenesis: Mitochondrial DNA replication increases in distal axons as an early response to Parkinson's disease-relevant stress. J. Neurosci. 0541–18.

91. Wong, Y.C., and Holzbaur, E.L.F. (2015). Temporal dynamics of PARK2/parkin and OPTN/optineurin recruitment during the mitophagy of damaged mitochondria. Autophagy *11*, 422–424.

92. Youle, R.J., and Karbowski, M. (2005). Mitochondrial fission in apoptosis. Nat. Rev. Mol. Cell Biol. *6*, 657–663.

93. Yu, T., Robotham, J.L., and Yoon, Y. (2006). Increased production of reactive oxygen species in hyperglycemic conditions requires dynamic change of mitochondrial morphology. Proc. Natl. Acad. Sci. U. S. A. *103*, 2653–2658.

94. Zhao, S., Fortier, T.M., and Baehrecke, E.H. (2018). Autophagy Promotes Tumor-like Stem Cell Niche Occupancy. Curr. Biol. *28*, 3056-3064.e3.

95. Zhen, Y., Spangenberg, H., Munson, M.J., Brech, A., Schink, K.O., Tan, K.-W., Sørensen, V., Wenzel, E.M., Radulovic, M., Engedal, N., et al. (2019). ESCRT-mediated phagophore sealing during mitophagy. Autophagy 1–16.

Appendix

Appendix 1.1: Loss of Gfzf, a conserved glutathione S-transferase, led to Marf-dependent increase in mitochondrial length and decrease in mitochondria number in axons.

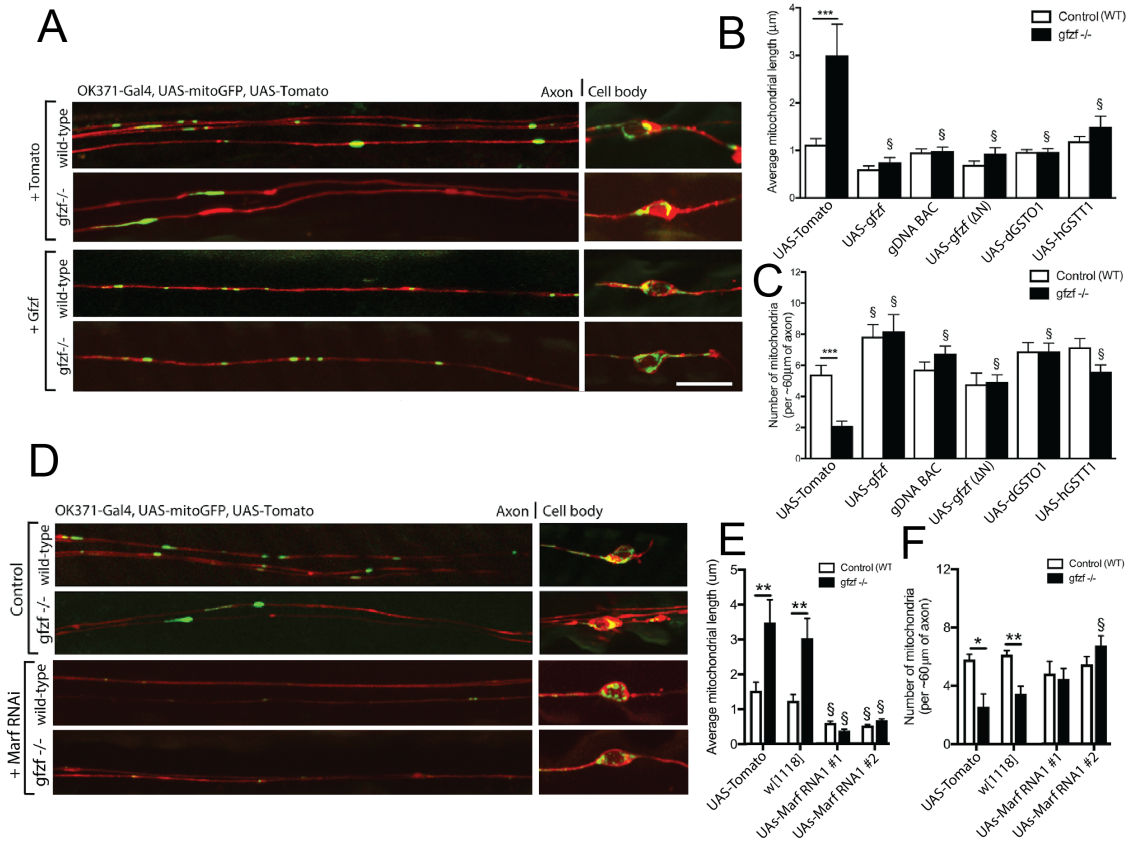

Appendix 1.1:

The data showed above were adapted from *Smith and Lin et al., Neuron 2019* (doi: 10.1016/j.neuron.2019.04.017). Homozygous mutant neurons were generated, labeled and imaged the same way as in Fig. 2.1. **(A-C)** *gfzf*-mutant phenotype—increased mitochondrial length and reduced mitochondrial number—was rescued by re-expression of *gfzf* cDNA construct (UAS-gfzf), full-length of *gfzf* (gDNA BAC), *gfzf* with only the GST domain (UAS-gfzf ΔN), and other GST-containing genes such as *Drosophila* dGSTO1 in and human hGSTT1. **(D-F)** This mutant phenotype was also rescued by knocking down *marf*, a Mitofusin homolog that drives mitochondrial fusion, via two independent RNAis, suggesting that the mitochondrial length increase in *gfzf*-mutant axons is the result of excessive mitochondrial fusion. At least 10 wings (one wing/animal were examined in each genotype ($N \geq 10$). Scale bar: 10 μm. Data were analyzed via 2-way ANOVA. *$p>0.05$ and **$p>0.01$ between genotypes following the same treatment; $^{\S}p>0.05$ and $^{\S}p>0.01$ between experiment groups and their respective baseline controls. Data were expressed as mean ± SEM.

Appendix 1.2: Gfzf-dependent mitochondrial fusion was caused by GSH:GSSG imbalance

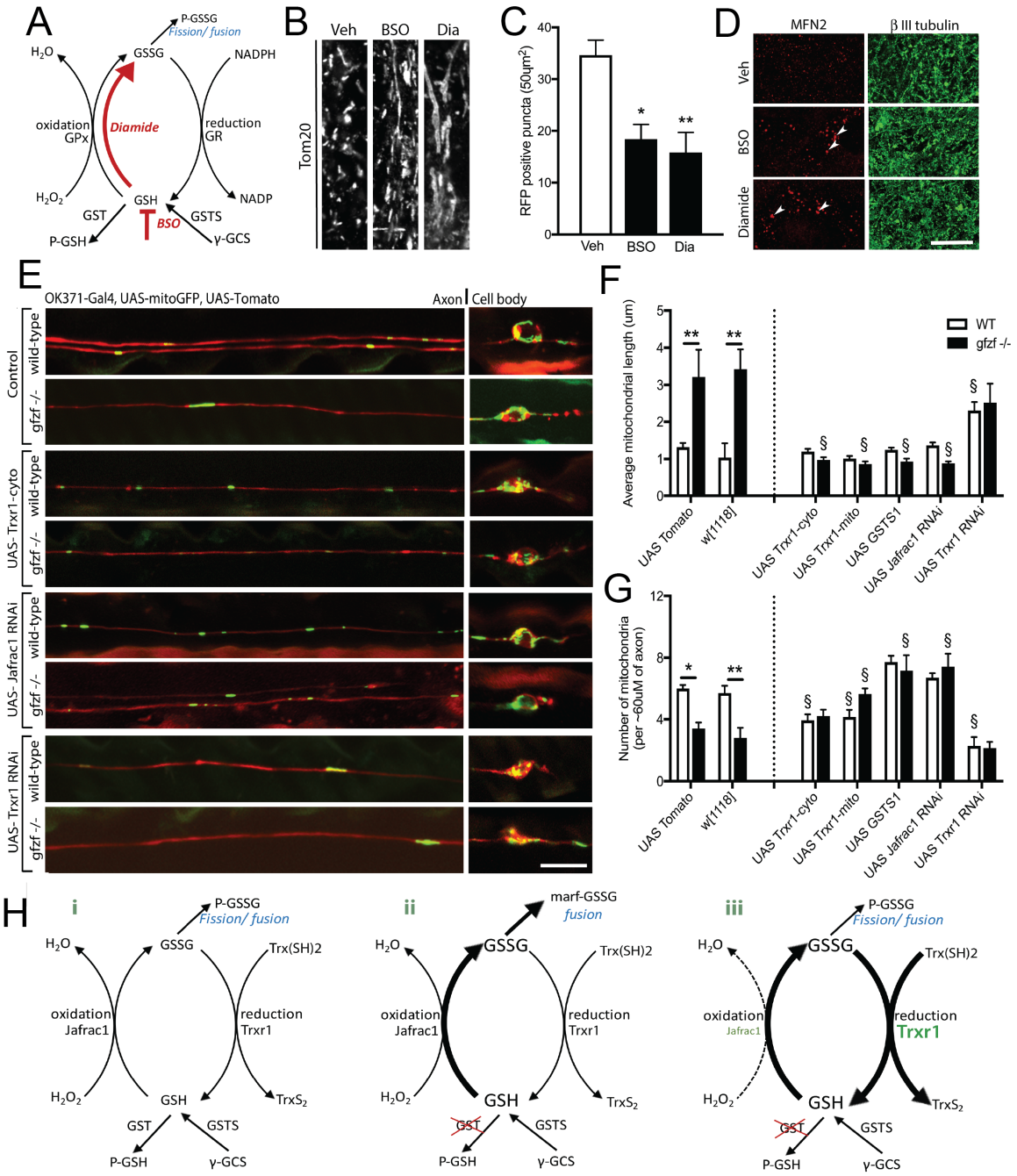

Appendix 1.2:

The data showed above were adapted from *Smith and Lin et al., Neuron 2019* (doi: 10.1016/j.neuron.2019.04.017). **(A)** A diagram illustrating the effect of pharmacological treatments of Dia (Diamide, 100μM) and BSO (L-buthionine-sulfoximine, 600μM) on the glutathione pathway—decrease in GSH:GSSG ratios. **(B-D)** Both treatments to 3-week-old primary cortical neurons led to increase in mitochondrial length (B, C) and oligomerization of Mfn2 (D). **(E-G)** Rescue of mitochondrial length (quantified in F) and number (quantified in G) was achieved by overexpression of a reductase TrxR1 (UAS Trxr-cyto and UAS Trxr-mito) or knockdown of a specific oxidase Jafrac1 (UAS Jafrac RNAi); in addition, knockdown of TrxR1 increased mitochondrial length, recapitulating *gfzf*-knockout phenotype. **(H)** A diagram showing how Gfzf acts synergistically with Jafrac1 and TrxR1 for GSH:GSSG and fission-fusion balance (i). GST ablation was found to alter this balance in favor of increased mitochondrial fusion (ii); however, reducing levels GSSG by increasing levels of TrxR1 restores this imbalance (iii). Following the loss of GSTs, GSH increases and is rapidly turned into GSSG, leading to axonal GSSG accumulation, which in turn leads to subsequent Mfn oligomerization and mitochondrial fusion. At least 10 wings (one wing/animal were examined in each genotype ($N \geq 10$). Scale bar: 10 μm. Data were analyzed via 2-way ANOVA. *$p>0.05$ and **$p>0.01$ between genotypes following the same treatment; $^{\S}p>0.05$ and $^{\S}p>0.01$ between experiment groups and their respective baseline controls. Data were expressed as mean ± SEM.